Age Constraints on Late Mesozoic Lithospheric Extension and Origin of Felsic Volcanism in the Songliao Basin, NE China

Shuang-Qing Li,[1] *Yi-Zeng Yang,*[1] *Qing-Lu Xie,*[2] *Yan Wang,*[1] *and Fukun Chen*[1,*]

1. Chinese Academy of Sciences Key Laboratory of Crust-Mantle Materials and Environments, School of Earth and Space Sciences, University of Science and Technology of China, Hefei, China; 2. Bengbu Naval Petty Officer Academy, Department of Navigation, Bengbu, China

ABSTRACT

Late Mesozoic lithospheric extension in NE Asia resulted in the development of a large extensional province and widespread formation of volcanosedimentary basins. Songliao basin is the biggest in that region, situated between the Siberian and Sino-Korean (North China) cratons. The Songliao basin contains voluminous volcanic rocks as a major part of the basin fill. Volcanic successions form a significant but unexposed part of the late Mesozoic magmatic province in NE China. Here we report zircon U-Pb ages and geochemical data for felsic volcanic rocks from the Songliao basin. Zircon populations of two types of rhyolites with distinct I- and A-type affinities, analyzed by laser ablation inductively coupled plasma mass spectrometry, yielded similar U-Pb ages of 114 ± 2 and 113 ± 2 Ma, respectively. Whole-rock Nd and zircon Hf isotope data of the felsic rocks indicate an origin from newly formed crustal protoliths. The I-type dacites and rhyolites show geochemical signatures with subduction-related affinity, indicating generation by partial melting of juvenile crust that originated from melting of subduction-modified mantle sources, whereas the A-type rhyolites have higher heavy rare earth element and high field strength element concentrations and lower Ba/Nd ratios that are interpreted as evidence for melting of I-type felsic lower crustal sources in an intraplate tectonic environment. Typical geochemical compositions of A-type rhyolites indicate anorthite-rich plagioclase as a residual magmatic phase and imply melting at shallow crustal levels. The A-type felsic rocks were generated during a period of maximum lithospheric extension below eastern China around 110 Ma, and this thinning process was probably related to the retreat of the Paleo-Pacific trench.

Online enhancements: supplementary tables.

Introduction

Northeast China located between the Siberia and North China cratons comprises a Paleozoic orogenic collage that is traditionally considered the eastern segment of the Central Asian Orogenic Belt (CAOB). Major parts of eastern China and eastern Mongolia experienced lithospheric extension during the late Jurassic and early Cretaceous, and these processes drove the formation of a basin-and-range province (Li et al. 1995; Ren and Li 1998; Ren et al. 2002). The basins display a remarkable diversity of style and size and vary from low-strain extensional basins, to transtensional basins, to rapidly filled basins associated with high-strain extensional metamorphic core complexes (Wang et al. 2011, 2012; Graham et al. 2012). Late Mesozoic granitoids and volcanic rocks are also widespread along the East Asian continental margin, and their generation has been discussed in the geological literature over the past decades (e.g., Itsikson et al. 1965; Li et al. 1995, 2014*a*; Sokolov et al. 1999; Liu et al. 2001; Wang et al. 2006*a*; Zhang et al. 2010). Due to the diversity of the igneous assemblages, different models on the Mesozoic tectonic setting of NE China have been proposed (e.g., Wang et al. 2006*a*; Zhang et al. 2010; Wu et al. 2011*a*; Xu et al. 2013). Temporal relations between the magmatic activities are still obscure, partly due to the fact that inconsistent ages have been obtained on the same igneous formation by different geochronological methods (e.g., Wang et al. 2002*a*, 2002*b*; Zhang et al. 2011; Xu et al. 2013). To

Manuscript received November 11, 2014; accepted March 10, 2015; electronically published April 21, 2015.

* Author for correspondence; e-mail: fkchen@ustc.edu.cn.

[The Journal of Geology, 2015, volume 123, p. 153–175] 0022-1376/2015/12302-0004$15.00. DOI:10.1086/681600

better understand the generation of the late Mesozoic igneous rocks and their tectonic affinities, representative samples need to be examined with adequate isotopic and geochronological methods.

The Songliao basin is the most important oil- and gas-bearing basin of China. Voluminous late Mesozoic volcanic rocks are covered by an Albian to Maastrichtian sedimentary succession, up to 6 km in thickness (Wang et al. 2006*b*). Geochronological data indicate a long-lasting magmatic evolution from ca. 158 to 113 Ma (Wang et al. 2002*a*). Other dating results suggest that the peak of volcanic activity occurred during the late Cretaceous (Xu et al. 2013). Geochemical data and field observations of the extension-related volcanic rocks have documented a variety of compositions (e.g., Meng et al. 2013), reflecting the complexity of magma sources. This study confirms the presence of two types of felsic volcanic rocks in the Songliao basin with distinct compositional characteristics that allow us to constrain different magma sources and to make inferences about the temporal variation of lithospheric extension in this area.

Geological Setting and Sample Description

The Songliao basin, located on the eastern part of the CAOB, covers an area of 260,000 km^2 and is the most prolific oil- and gas-producing basin in northern China (e.g., Sengör et al. 1993; Dobretsov et al. 1995; Xiao et al. 2003; Windley 2007; fig. 1*a*). It is situated to the south of the Mongol-Okhotsk suture that closed at 160–140 Ma (e.g., Zorin 1999). In its present configuration, the Songliao basin is delimited by major faults and surrounded by mountain ranges that are mainly composed of Phanerozoic granites (Wu et al. 2011*a*; Ge et al. 2012; fig. 1). The depth to the Moho ranges from ~27 km beneath the depression to more than 42 km below the surrounding mountains and tilts northwestward, with the shallowest and deepest Moho being located at the eastern flank of the basin and the Great Xing'an range (Tao et al. 2014; fig. 1*a*). The deep-seated mantle high beneath the Songliao basin strikes NNE and coincides with the overlying Cretaceous depression (Li et al. 2012).

Basement rocks within and around the Songliao basin comprise Paleozoic marine metasediments, andesites, and granites. Some gneisses and schists were assigned to be Precambrian in age (Wang et al. 1993). Recent studies, however, have shown that Precambrian rocks are actually absent beneath the Songliao basin and the gneisses and schists are mainly deformed Paleozoic magmatic rocks. Nevertheless, whether Precambrian basement rocks occur is still a matter of debate (e.g., Pei et al. 2007, 2008; Wang and Wang 2007; Wang et al. 2007; Yu et al. 2008; Zhang et al. 2008*b*; Wu et al. 2011*a*).

The basin sequence shows evidence for three main tectonic stages, that is, early rift, middle sag, and late inversion (Song 1997; Ren et al. 2002; Wang et al. 2002*b*). During the early-rift stage, normal faulting and episodic volcanic eruptions lead to the growth of several discrete NE-SW- and NNE-SSW-trending rift basins. Basin fill consists of the late Jurassic to early Cretaceous Huoshiling and early Cretaceous Shahezi and Yingcheng (JBGMR 1988; Xu et al. 2013) Formations. Deposition of the Huoshiling and Yingcheng Formations was concomitant with substantial volcanic activity, whereas the Shahezi Formation contains abundant alluvial-lacustrine sediments. The intense volcanic activity ceased after the syn-rift phase. In the late Cretaceous sag stage, tectonic activity decreased and basin-infill strata progressively onlapped the basin margin and were deposited in a broad downwarped lacustrine depression. Near the end of the late Cretaceous, inversion of the basin occurred on NE- and NNE-trending faults, with alternating anticlinal and synclinal trends. The area of the lacustrine basin was significantly reduced and elevated to its present topographic position.

In the study area, late Mesozoic volcanic rocks (Huoshiling and Yingcheng Formations) were erupted or emplaced over large areas in an evolving basin-and-range setting (Graham et al. 2012). Drill cores from the Songliao basin indicate that these rocks are widespread at a depth between 1500 and 4800 m, with volcanic horizons tens of meters to 1000 m thick interlayered with sedimentary strata (Wang et al. 2002*b*; Zhang et al. 2011). The volcanic rocks are dominated by felsic volcaniclastic rocks, with minor mafic-intermediate rocks that comprise basalts, basaltic andesites, andesites, and rare trachyandesites. The felsic volcanic rocks are mainly rhyolites and dacites.

Data from drill cores indicate that volcanic rocks of the Huoshiling Formation are mainly distributed in the southeastern part of the Songliao basin. This formation represents the earliest syn-rift strata. Previous $^{40}Ar/^{39}Ar$ dating on drill-core samples yielded late Jurassic (158–147 Ma) ages (Wang et al. 2002*a*, 2002*b*), but recent U-Pb zircon dating on trachyandesite and andesite of the Huoshiling Formation indicates early Cretaceous ages (133–129 Ma; Pei et al. 2008). Felsic volcanic rocks of the Yingcheng Formation are widespread in the Songliao basin and are exposed along its eastern margin (fig. 1*b*). U-Pb dating of zircons yielded crystallization ages of 120–110 Ma in the northern part of Songliao basin (Ding

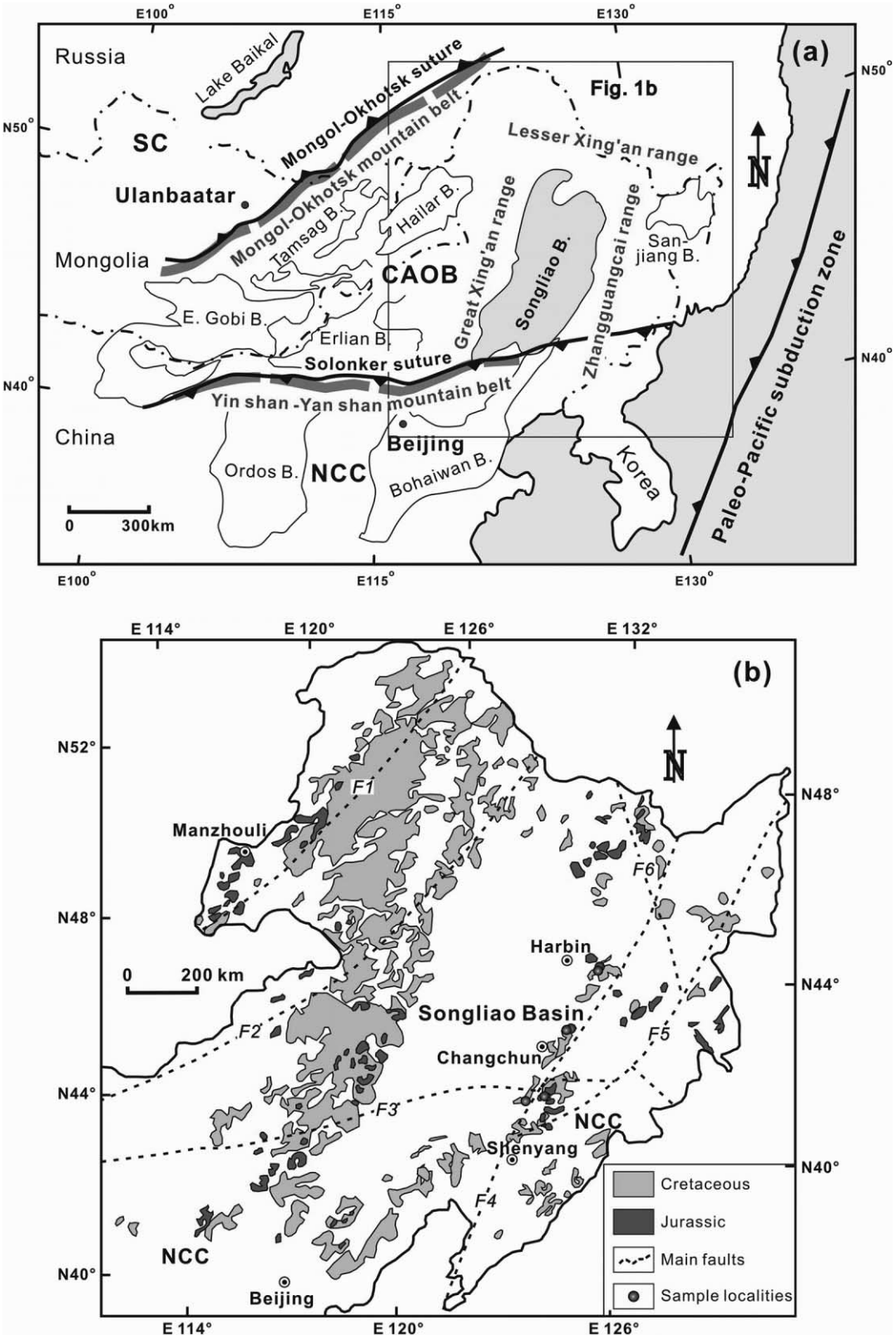

Figure 1. *a*, Geological map of NE China showing the location of the study area in the Central Asian Orogenic Belt (CAOB) and bordering Mongol-Okhotsk and Solonker sutures. The major late Mesozoic volcanosedimentary basins in the CAOB and bordering cratons are outlined. SC = Siberian craton; NCC = North China craton. Map simplified from Meng (2003) and Wang et al. (2011); sutures and subduction polarities from Ritts et al. (2001) and Wang et al. (2011). *b*, Map showing the Songliao basin and distribution of Mesozoic volcanic rocks in NE China (modified after Li et al. 2012; Xu et al. 2013). F1 = Yayuan-Ximutu fault; F2 = Hegenshan-Heihe fault; F3 = Solonker-Xra Moron fault; F4 = Yitong-Yilan fault; F5 = Dunhua-Mishan fault; F6 = Mudanjiang fault. Sample localities are indicated. A color version of this figure is available online.

et al. 2007; Zhang et al. 2007, 2008*a*; Jin et al. 2011) and 119–109 Ma in the southern part of the basin (Pei et al. 2008; Zhang et al. 2011). These ages (i.e., 120–109 Ma) are younger than previously reported $^{40}Ar/^{39}Ar$ ages (136–113 Ma) on drill-core samples (Wang et al. 2002*a*, 2002*b*).

In this study, we analyzed 23 felsic rock samples and zircons of two different types of dacites/rhyolites. Dacites and rhyolite samples are porphyritic rocks with phenocrysts of plagioclase (oligoclase), sanidine, quartz, biotite, and more rarely amphibole and account for approximately 10%–20% of the rocks by volume. The phenocrysts are submerged into an aphanic or microspherulitic groundmass consisting of completely recrystallized glass with rare plagioclase laths and small quartz grains. Flow banding and spherulitic and perlitic textures are common.

Analytical Methods

Zircon U-Pb Dating and Trace Element Analyses. The zircon concentrates were isolated from crushed rocks by standard magnetic- and heavy-liquid mineral separation techniques. More than 100 zircon grains of each sample were handpicked under a binocular microscope for analysis. Selected crystals were transparent, colorless, and mostly subangular, with some grains showing well-defined prisms and euhedral to subhedral habitus. The zircons then were mounted on adhesive tape, embedded in epoxy resin, and polished to about half of their thickness to expose their inner structure. Cathode luminescence (CL) images were taken with a Cameca SX-50 microprobe at the Institute of Geology and Geophysics, Chinese Academy of Sciences (IGG-CAS), Beijing. Zircon U-Pb isotopic compositions and trace elements were analyzed at the Key Laboratory of Crust-Mantle Materials and Environments at the University of Science and Technology of China (USTC), Hefei. We used an inductively coupled plasma mass spectrometer (ICP-MS; Perkin Elmer Elan DRC II) equipped with a Microlas system (GeoLas 200M, 193 nm ArF-exc imer laser). The analyses were carried out with a pulse rate of 10 Hz, beam energy of 10 J/cm^2, and spot diameter of 60 μm, sometimes 30 μm where necessary. Signal and background measuring times were 70 and 40 s, respectively. Age calculations were calibrated against Zircon 91500 reference material analyzed after every fifth sample spot. In order to avoid an age bias due to selective analysis of a certain type of zircon and specific zircon domains, cores and rims of more than 20 grains of different sizes were randomly analyzed. More details on the laser ablation U-Pb dating technique are given in Liu et al. (2007). The conventional correction procedure for common lead could not be used due to the low ^{204}Pb signal and interfering ^{204}Hg from Ar. Instead, we used the procedure "ComPbCorr#3_18" of Andersen (2002), which solves for the mass balance caused by the combined effects of common lead and lead loss at a specific time. The U-Pb raw data were processed with Glitter 4.0 (Macquarie University, Sydney, Australia), and the U-Pb ages were calculated with ISOPLOT 3.0 (Ludwig 2003). During the course of this study, 17 spots analyzed on Zircon 91500 yielded a mean $^{207}Pb/^{206}Pb$ age of 1065 ± 50 Ma (2 SD) and a mean $^{206}Pb/^{238}U$ age of 1062 ± 9 Ma (2 SD). Here we report the ages of the $^{238}U/^{206}Pb$ system because of its high precision for young rocks. The analytical data are listed in table S1 (tables S1–S3 available online).

Element concentrations of zircons were calibrated against the NIST610 reference material, which was measured twice every 10 sample spots. The internal standard was stoichiometric Si for zircon. During time-resolved analysis, contamination resulting from inclusion and fractures was monitored by different elements, the corresponding part of the signal was excluded, and spikes in time-resolved signals were filtered. We note that contaminations from microinclusions whose signal spread over the entire analysis cannot be eliminated with this procedure. The results were processed using the macro program LaTEcalc.xls written in Excel spreadsheet software. The detailed analytical procedure follows Yuan et al. (2004). Precision and accuracy of the NIST-610 analyses range from 2% to 5% for rare earth elements (REE), Y, Rb, Sr, Nb, Ta, Hf, Th, and U at parts per million concentration level and from 8% to 10% for P, Ti, and Pb. The analytical data are listed in table S2.

Identification of Mineral Inclusions. Mineral inclusions in zircons were identified by laser Raman microscopy (Thermo Scientific; Nicolet, DXR) at USTC Hefei. This analysis was carried out to identify zircons suitable for further analysis. The measured laser power of the 532-nm excitation line of the Nd:YVO_4 laser was 24 mW on the sample with a ~1-μm spot size. The aperture was 25-μm pinhole. Raman spectra were collected in four accumulations of 8 s each in the range of 100–3500 cm^{-1} in steps of 3 cm^{-1}. Monocrystalline silicon and polystyrene were analyzed during the analytical session to monitor the precision and accuracy of the Raman data.

Whole-Rock Major and Trace Elements. Whole-rock samples were crushed and chips free of weathered material and amygdules were ground in a tungsten-carbide mill. Major-element concentrations were determined on glass tablets at IGG-CAS Beijing with wavelength-dispersive X-ray fluorescence spectrom-

etry (SHIMADZU XRF 1500 spectrometer; method described in Guo et al. 2006). Loss on ignition (LOI) was determined on ca. 5 g of sample powders baked at 1000°C for 10 h. Precision of the major-element concentrations is ≤3%, and the accuracy as determined on the Chinese whole-rock standard GSR-1 is ~5%.

For trace-element analysis the sample powders were decomposed in a mixture of Hf and HNO_3 in high-pressure Teflon bombs for 2 d. The sample solutions were analyzed with the Elan DRC-II-ICP-MS at USTC using the procedures described in Hou and Wang (2007). Ruthenium was used as an internal standard to correct for matrix effects and instrument drift. The total procedure blank of <35 ng for all elements is insignificant compared to the analyzed element concentrations. The precision of the trace element data is ~5%, and the accuracy of the data is ≤5% for most elements as estimated from analyses of the USGS rock standards BHVO-2 and AGV-2.

Whole-Rock Sm-Nd Isotopes. The Sm-Nd isotopic analyses were carried out at Ludwig-Maximilians-Universität (LMU) Munich according to the methods described in Hegner et al. (1995). Sm and Nd concentrations were determined by isotopic dilution using ^{149}Sm and ^{150}Nd tracers. The isotopic abundance ratios were determined on an upgraded MAT 261 mass spectrometer. $^{143}Nd/^{144}Nd$ ratios are normalized to $^{146}Nd/^{144}Nd = 0.7219$ and Sm isotopic ratios to $^{147}Sm/^{152}Sm = 0.56081$ using a Rayleigh fractionation law. During the course of this study, analyses

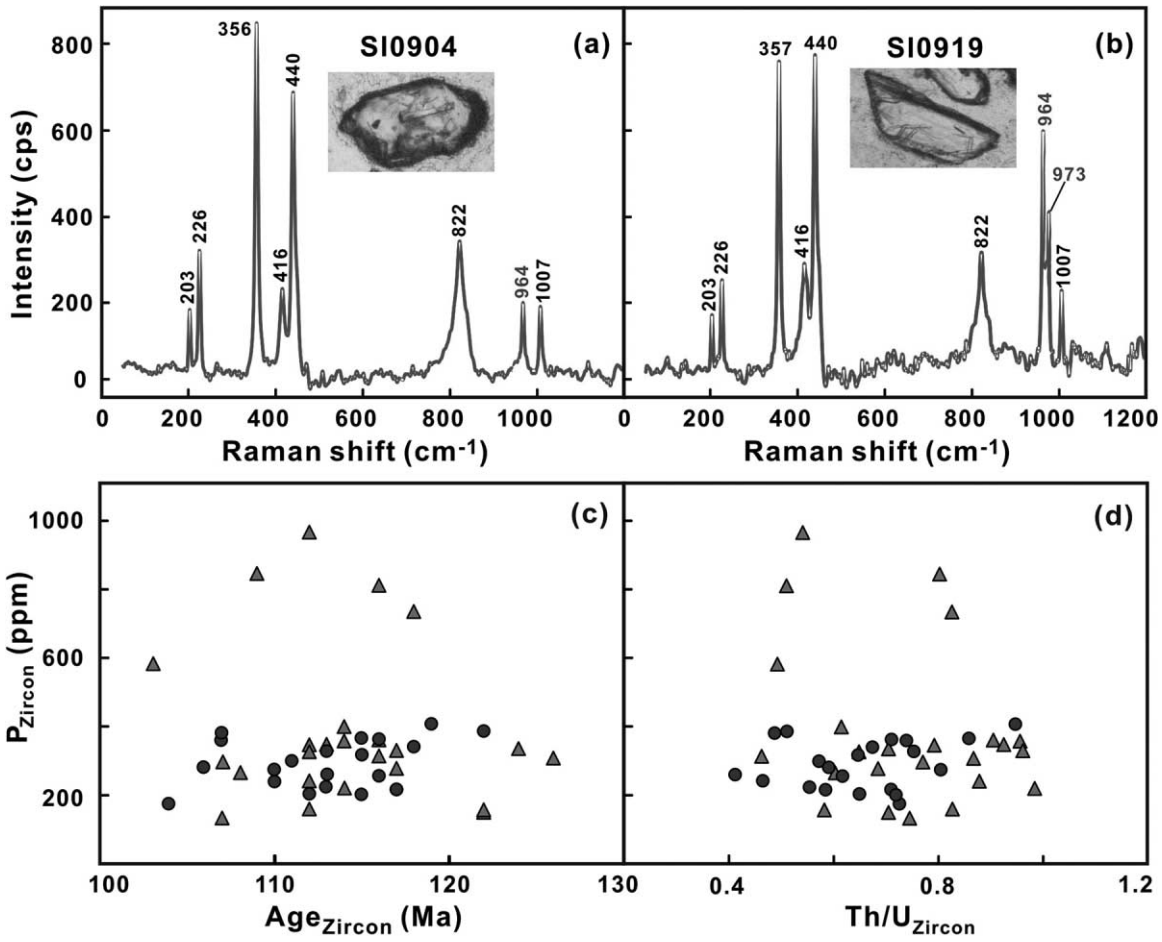

Figure 2. Representative laser Raman spectra of apatite inclusions (964 cm^{-1}) in zircon from A-type rhyolite (*a*) and apatite and monazite (973 cm^{-1}) inclusions in zircon of I-type rhyolite (*b*). Note that the spectra contain host zircon peaks at 201–203, 223–226, 354–358, 415–443, 822, and 1007–1008 cm^{-1}. In situ zircon U-Pb age versus P concentration (*c*) and Th/U ratio versus P concentration (*d*) in zircons of felsic volcanic rocks from Songliao basin. Triangles = zircon grains from I-type felsic volcanic rocks; circles = zircon grains from A-type rhyolites (see fig. 6 for felsite classification). A color version of this figure is available online.

of the JND (Tanaka et al. 2000) at LMU yielded $^{143}Nd/^{144}Nd = 0.512100 \pm 0.000006$ (2σ, $n = 8$).

Zircon Lu-Hf Isotope Analysis. We measured Hf isotopic composition of the zircons that had been used for U-Pb and trace element analyses. Laser ablation multicollector inductively coupled plasma mass spectrometry (LA-MC-ICP-MS) Lu-Hf isotope analysis was carried out at IGG-CAS Beijing. Instrumental conditions and data acquisition followed Wu et al. (2006). A GeoLas-193 laser ablation microprobe was attached to a Neptune multicollector ICP-MS. During analyses, spot sizes of 60 μm with a laser repetition rate of 10 Hz at 100 mJ were used. Both He and Ar carrier gases were used to transport the ablated sample from the laser ablation cell via a mixing chamber to the ICP-MS torch. During analytical processes, the $^{176}Hf/^{177}Hf$ ratios of standard zircons Mud Tank and GJ-1 were 0.282515 ± 4 (2σ, $n = 90$) and 0.282021 ± 5 (2σ, $n = 54$), respectively, in good agreement with the recommended values (Jochum et al. 2005).

Analytical Results

Apatite Inclusions in Zircons. Numerous mineral inclusions were found in the investigated zircons. Most of them have long columns with a width-to-length ratio of 1:10 to 1:5. The in situ microlaser Raman analyses reveal peaks at around 964 and 973 cm^{-1}, which can be assigned to the typical peak positions of apatite and monazite (fig. 2*a*, 2*b*). Since most in situ analyses of zircons could not avoid such inclusions that show variable high light REE (LREE) and P (figs. 2*c*, 2*d*, 9*b*) concentrations, it is necessary to evaluate the influence of apatite inclusions on the precision of zircon U-Pb dating and trace element composition. As shown in figure 2*c* and 2*d*, there is no correlation between P concentration, single zircon age, and Th/U ratio, indicating that the effect of apatite inclusions on the analytical results (except for LREE) is negligible.

Zircon U-Pb Ages. LA-ICP-MS zircon-spot ages for two rhyolites from the Yingcheng Formation are shown in figure 4, and the U-Pb isotope ratios and corresponding ages are given in table S1. Zircon grains from the two rhyolitic samples are colorless and transparent; some show well-defined prism faces and appear to have largely retained their euhedral to subhedral crystal shapes. CL images reveal that the zircon crystals show well-developed oscillatory zoning and lack any inherited cores (fig. 3). Th/U ratios of >0.4 (table S2) are characteristic of an igneous origin (Hanchar and Hoskin 2003). It is noticeable that zircons from sample SL0904 show less regular

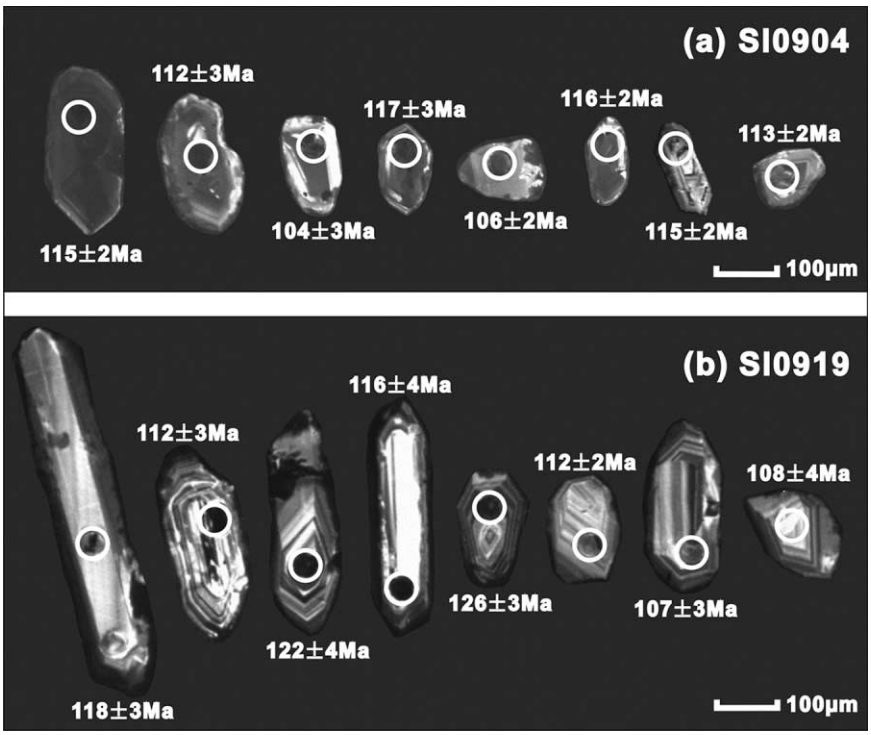

Figure 3. Cathode luminescence images of selected zircon grains from A-type rhyolite (sample SL0904; *a*) and I-type rhyolite (sample SL0919; *b*). Circles indicate the analyzed domains and the corresponding average $^{238}U/^{206}Pb$ age obtained by laser ablation inductively coupled plasma mass spectrometry with 1σ error.

oscillatory zoning and crystal shapes, compared to zircon crystals from sample SL0919 (fig. 3). In the following, the age results of these samples are described according to their lithology.

Sample SL0904 was collected from the type section of the Yingcheng Formation, located at Guanma Mountain, Jiutai City, Jilin Province (lat 44°23′13.6″N, long 126°08′10.8″E). In this profile, a large rhyolite is exposed, containing compact rhyolites and effusive rhyolites with lithophyses, flow banding, and vesicles. The sample for zircon U-Pb dating was taken from the uppermost section of the profile. Twenty-one concordant zircons out of 24 in total gave within-error data points with $^{206}Pb/^{238}U$ ages ranging from 122 ± 6 (2σ) to 104 ± 6 (2σ) Ma (table S1), with a weighted mean age of 113 ± 2 Ma (2σ; MSWD = 3.3, n = 21; fig. 4*a*).

Sample SL0919 was collected from a rhyolitic porphyry layer ~10 km northeast of the Guanma Mountain profile. Rocks in this area consist of basaltic-andesite, andesite, volcanic breccia, perlite, dacite, rhyolite, and tuff. The $^{206}Pb/^{238}U$ ages of 24 zircon grains out of 28 in total are concordant within error and range from 126 ± 6 (2σ) to 103 ± 10 (2σ) Ma (table S1), with a weighted mean age of 114 ± 2 Ma (2σ; MSWD = 2.4, n = 24; fig. 4*b*).

Mean zircon ages of samples SL0904 and SL0919 overlap within error (fig. 4) and are interpreted as the crystallization age of the rhyolitic rocks. Considering that both samples were collected from the upper Yingcheng Formation, their ages can be correlated with the fade out of Mesozoic volcanic activity in the Songliao area. Thus, the results constrain not only the time of lava eruption but also the final stage of the volcanic activity.

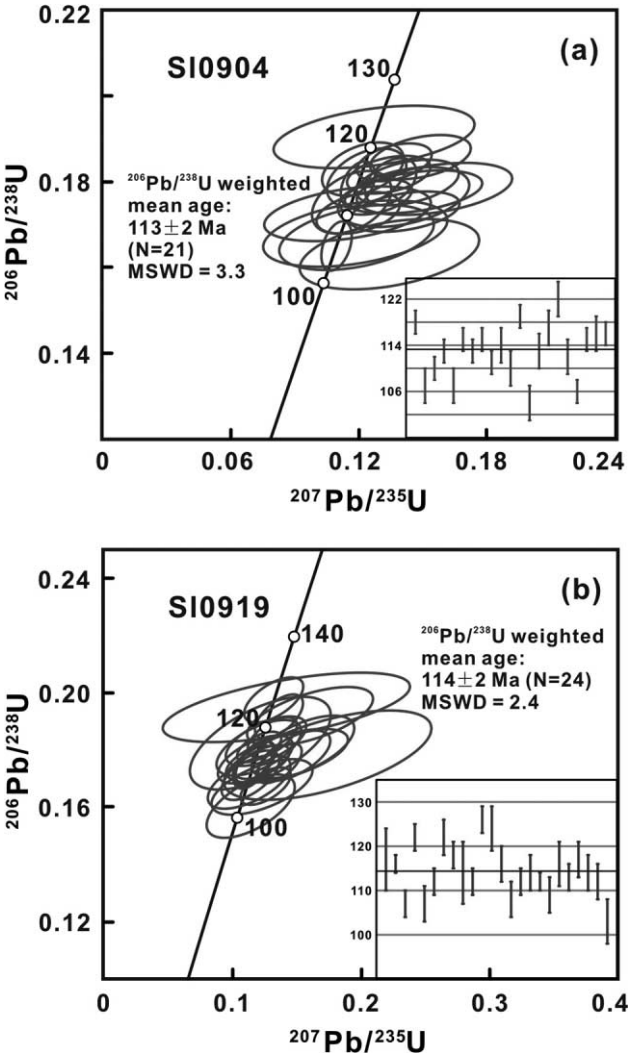

Figure 4. Concordia diagrams for laser ablation inductively coupled plasma mass spectrometry zircon analyses of late Mesozoic A- and I-type rhyolites from the Songliao basin. Error envelopes indicate 1σ age uncertainties. A color version of this figure is available online.

Whole-Rock Geochemistry and Zircon Trace Elements. Major- and trace-element data for 27 early Cretaceous rhyolitic rocks from the Songliao basin are listed in tables 1, 2. LOI ranges from 0.26 to 1.38 wt%. The rocks plot as dacites and rhyolites on a SiO_2 versus Na_2O+K_2O classification diagram (Le Bas et al. 1986; fig. 5) and show K_2O/Na_2O ratios >1, except two samples (FK11-114, FK11-116) that have high Na_2O concentrations (tables 1, 2). SiO_2 concentrations range from 66 to 83 wt%. According to the geochemical characteristics, the volcanic rocks can be divided into I-type dacites and rhyolites and A-type rhyolites (fig. 6*a*). Including data from literature (Meng et al. 2010, 2013; Zhang et al. 2011), the A-type rhyolites belong to the A1 subtype (fig. 6*b*), according to Eby (1992), which represents basaltic differentiates emplaced during continental rifting or intraplate magmatism.

Further geochemical relationships between the I- and A-type rocks are shown in figure 7. Both suites show negative correlations between SiO_2 and Al_2O_3 concentrations, indicating the presence of plagioclase fractionation during magma differentiation. The presence of different heavy REE (HREE)–rich minerals such as zircon and/or hornblende might have led to different fractionation trends in the SiO_2 versus HREE concentration diagram (fig. 7*c*). Phosphor content remains constant with increasing silica (fig. 7*b*), but the A-type rhyolites show much lower P concentrations compared to the I-type dacites and rhyolites. Similarly, the A-type rhyolites have higher HREE and high field strength element (HFSE) and lower Al_2O_3,

Table 1. Major Element (wt%) and Trace Element (ppm) Concentrations for I-Type Felsic Rocks of Songliao Basin, NE China

Sample	FK11-125	FK11-119	FK11-118	FK11-117	FK11-120	FK11-114	FK11-115	FK11-116	SL0917	FK11-109	FK11-110	FK11-108	FK11-124	FK11-123
SiO_2	65.90	70.02	70.47	70.69	71.03	71.20	72.69	72.72	74.05	74.68	75.28	75.84	76.10	76.25
TiO_2	.80	.43	.41	.42	.41	.32	.31	.32	.28	.26	.26	.24	.08	.08
Al_2O_3	14.75	15.03	14.79	14.89	14.56	15.40	14.09	14.86	13.43	12.30	12.05	11.50	12.95	12.71
$Fe_2O_3^{t}$[a]	4.66	2.30	2.16	2.12	2.27	1.58	1.71	1.21	1.61	1.61	1.72	1.84	1.01	1.40
MnO	.09	.06	.05	.06	.06	.06	.06	.03	.01	.03	.03	.03	.01	.04
MgO	2.50	.40	.37	.42	.42	.19	.22	.17	.39	.25	.34	.36	.09	.10
CaO	4.12	1.50	1.34	1.46	1.21	.24	.47	.20	1.27	.43	.72	.32	.26	.23
Na_2O	2.12	3.69	3.56	3.72	3.76	5.97	3.62	4.94	3.42	1.73	2.09	1.36	3.37	3.34
K_2O	3.16	4.84	5.13	4.94	4.95	2.83	5.15	4.21	4.92	7.86	6.54	7.93	5.06	4.78
P_2O_5	.28	.07	.06	.06	.07	.05	.04	.05	.08	.07	.08	.06	.02	.02
LOI	.78	.40	.62	.26	.62	.90	.92	.76	.49	.60	.64	.66	.62	.76
Total	99.16	98.74	98.96	99.04	99.36	98.74	99.28	99.47	99.96	99.82	99.75	100.14	99.57	99.71
Mg#[b]	52	26	26	28	27	19	20	22	33	24	28	28	15	13
Sc	9.8	3.5	3.0	3.1	3.0	2.5	2.3	2.3	1.84	1.91	1.88	1.71	.53	.52
V	164	147	119	245	223	142	197	141	22	114	174	164	155	155
Cr	150	135	110	221	202	129	180	128	67	106	159	150	142	142
Co	3.0	2.1	1.67	2.4	5.0	1.77	1.85	1.51	7.6	2.4	3.1	2.6	1.58	1.83
Ni	10.6	6.6	5.3	7.4	13.3	5.1	5.4	4.1	4.9	6.2	7.9	6.7	4.0	4.7
Cu	55	21	31	24	38	21	33	39	5.3	20	21	20	20	15.0
Zn	80	47	80	68	65	36	71	51	25	28	46	73	41	65
Ga	17.6	15.5	15.9	15.9	16.7	15.4	16.0	16.3	13.9	12.0	13.8	12.2	13.4	14.3
Rb	84	123	128	126	141	63	121	102	96	164	144	162	184	171
Sr	432	104	104	107	101	108	111	96	257	85	179	61	28	37
Y	16.6	28	28	30	31	35	34	32	10.3	12.4	12.1	10.9	21	26
Zr	194	485	521	541	557	479	306	473	111	110	119	108	122	126
Nb	9.3	16.9	18.0	17.8	18.3	19.5	19.0	18.9	11.8	10.7	10.6	9.7	13.4	13.1
Cs	7.2	2.9	3.2	3.5	4.8	.63	1.76	1.53	1.29	4.4	3.9	3.3	4.9	3.5
Ba	536	873	872	855	867	645	945	881	494	444	484	403	473	390

La	28	35	36	39	42	33	43	27	24	28	27	25	26	32
Ce	59	72	78	83	88	90	92	103	41	54	52	47	57	67
Pr	6.9	8.1	8.5	9.1	9.6	8.5	10.1	6.8	4.6	5.5	5.2	4.8	5.9	7.0
Nd[c]	**28.02**	31	**34.42**	35	**34.98**	**32.11**	**39.25**	26	**17.67**	18.8	**17.13**	16.7	**22.99**	25
Sm[c]	**5.14**	6.0	**6.40**	6.6	**6.47**	**6.23**	**7.33**	5.4	**2.86**	3.2	**2.80**	2.8	**4.28**	4.8
Eu	1.50	1.20	1.12	1.22	1.17	1.20	1.29	1.01	.55	.57	.55	.47	.28	.28
Gd	4.4	5.3	5.5	5.9	5.9	5.9	6.6	5.1	2.3	2.7	2.5	2.4	3.6	4.4
Tb	.61	.84	.86	.91	.92	.97	1.05	.87	.33	.38	.37	.34	.59	.70
Dy	3.3	5.1	5.2	5.5	5.6	6.2	6.3	5.7	1.87	2.3	2.1	2.0	3.7	4.3
Ho	.61	1.00	1.02	1.09	1.09	1.26	1.24	1.20	.36	.44	.41	.38	.73	.84
Er	1.72	3.0	3.0	3.3	3.3	3.7	3.7	3.7	1.14	1.30	1.23	1.11	2.3	2.5
Tm	.25	.47	.49	.52	.52	.59	.57	.58	.180	.21	.191	.170	.37	.41
Yb	1.71	3.3	3.3	3.6	3.6	4.1	4.0	4.0	1.33	1.46	1.39	1.23	2.6	2.9
Lu	.26	.51	.52	.56	.56	.63	.61	.61	.21	.22	.22	.192	.41	.45
Hf	4.7	8.1	8.6	9.0	8.9	8.2	7.9	7.9	3.6	3.3	3.4	3.2	4.2	4.2
Ta	.63	1.31	1.41	1.42	1.42	1.48	1.44	1.41	.94	.97	.94	.88	1.43	1.38
Pb	9.3	20	26	20	32	21	24	29	21	32	29	17.7	34	12.0
Th	6.18	13.50	13.90	14.40	15.20	13.30	12.70	12.60	7.96	8.49	8.47	7.45	20	21
U	1.89	3.6	3.7	4.9	5.2	3.4	4.1	4.0	2.7	1.86	2.2	1.56	6.6	5.7
Nb/La	.33	.48	.51	.46	.44	.58	.44	.70	.50	.38	.39	.40	.52	.41
Eu/Eu*[d]	.93	.65	.59	.60	.56	.59	.56	.59	.66	.60	.61	.55	.22	.19
$(La/Sm)_N$	3.5	3.8	3.6	3.8	4.2	3.5	3.8	3.2	5.4	5.7	6.2	5.7	3.9	4.2
$(La/Yb)_N$	11.6	7.6	7.6	7.7	8.3	5.8	7.7	4.9	12.8	13.8	14.0	14.3	7.0	7.8

Note. LOI = loss on ignition; N = normalized to chondrite (Boynton 1984).

[a] Total Fe as Fe_2O_3.

[b] Mg# = 100 × molar $Mg^{2+}/(Mg^{2+} + TFe^{2+})$.

[c] Data in bold were determined by method of isotope dilution.

[d] $Eu/Eu^* = Eu_N/(Sm_N \times Gd_N)^{0.5}$.

Table 2. Major Element (wt%) and Trace Element (ppm) Concentrations for A-Type Rhyolites of Songliao Basin, NE China

Sample	FK11-93	FK11-95	FK11-94	SL0933	FK11-139	FK11-140	FK11-135	FK11-136	FK11-104	FK11-137	FK11-141	SL0902	FK11-138
SiO_2	75.26	75.51	75.83	76.79	78.31	78.32	79.01	79.52	80.39	81.27	81.98	82.35	82.54
TiO_2	.13	.13	.13	.14	.09	.09	.08	.08	.08	.07	.07	.07	.07
Al_2O_3	11.92	11.88	11.87	12.09	11.17	11.24	10.63	10.29	9.95	9.33	8.94	8.76	8.80
$Fe_2O_3^{t}$ [a]	2.96	2.50	2.48	1.71	1.40	1.01	1.08	1.24	1.32	.97	.99	.89	.94
MnO	.03	.04	.03	.01	.01	.01	.01	.01	.01	.00	.01	.01	.01
MgO	.18	.17	.13	.06	.07	.06	.07	.06	.06	.06	.06	.05	.07
CaO	.05	.11	.06	.08	.04	.04	.06	.07	.05	.04	.04	.07	.07
Na_2O	3.57	3.25	3.58	3.92	1.37	2.41	2.86	2.78	2.90	2.33	2.10	2.86	1.99
K_2O	4.74	4.68	4.72	4.68	6.24	5.31	4.91	4.86	4.54	4.61	4.81	4.51	4.76
P_2O_5	.01	.02	.02	.02	.03	.03	.02	.02	.02	.02	.01	.01	.02
LOI	.64	.88	.62	.49	1.38	.82	.58	.42	.34	.48	.50	.30	.58
Total	99.49	99.17	99.47	99.99	100.11	99.34	99.31	99.35	99.66	99.18	99.51	99.88	99.85
Mg# [b]	11	12	9	7	9	11	11	9	8	11	11	10	13
Sc	.97	.99	.98	.51	.59	.64	.61	.58	.56	.51	.52	.27	.49
V	163	164	192	.54	74	119	180	192	188	217	272	1.44	213
Cr	143	146	170	57	64	104	158	169	167	190	236	142	187
Co	1.28	1.67	1.86	7.7	1.14	1.44	1.92	1.90	1.83	2.1	2.2	6.8	2.9
Ni	3.1	3.8	4.4	1.72	2.7	3.4	4.5	4.6	4.3	4.8	4.8	3.5	7.1
Cu	81	69	91	2.5	30	18.0	29	40	35	16.3	16.2	1.60	20
Zn	110	71	100	53	28	40	58	53	58	51	47	27	52
Ga	27	26	27	24	18.8	23	20	18.1	20	16.3	16.8	14.9	15.0
Rb	201	204	205	195	398	363	217	216	209	198	213	197	201
Sr	7.9	13.9	11.6	8.2	2.5	3.1	4.2	4.4	4.1	5.0	5.0	9.5	6.8
Y	65	66	63	55	17.0	52	51	40	47	36	22	19.0	26
Zr	1077	1073	1095	519	605	663	693	659	424	585	537	335	553
Nb	54	62	52	53	47	44	42	40	36	37	33	33	36
Cs	1.89	2.0	2.2	2.4	2.9	3.5	3.1	3.1	3.8	2.5	2.8	3.1	2.7
Ba	15.2	18.8	15.1	11.2	65	56	34	30	18.9	41	39	36	50

La	85	83	85	43	25	45	39	31	43	26	27	26	35
Ce	170	164	163	90	76	97	89	74	88	65	63	63	89
Pr	18.2	18.5	18.4	10.8	6.5	11.5	9.6	8.0	10.9	6.7	6.7	6.2	9.1
Nd[c]	**63.03**	67	66	**45.22**	**34.84**	**40.39**	**35.68**	30	**37.31**	24	24	**21.26**	33
Sm[c]	**11.61**	12.7	12.4	**10.91**	**7.81**	**9.23**	**8.11**	6.9	**8.39**	5.7	5.3	**4.53**	7.4
Eu	.15	.15	.15	.14	.05	.04	.03	.02	.12	.03	.03	.02	.04
Gd	11.6	11.6	11.3	9.4	4.1	8.9	7.8	6.8	8.5	5.3	4.6	4.1	6.2
Tb	1.87	1.86	1.78	1.64	.65	1.53	1.37	1.20	1.42	.95	.80	.71	.98
Dy	11.8	11.6	11.1	10.0	3.8	9.6	8.8	7.4	8.8	6.2	5.0	4.3	5.7
Ho	2.3	2.3	2.2	2.0	.69	1.82	1.74	1.41	1.70	1.25	.97	.87	1.07
Er	6.9	6.7	6.4	5.9	2.0	5.2	5.0	3.9	4.9	3.7	2.9	2.7	3.1
Tm	1.12	1.07	1.00	.94	.29	.83	.76	.58	.77	.59	.48	.45	.48
Yb	7.4	7.1	6.6	6.4	2.0	5.4	5.0	3.8	5.1	4.1	3.3	3.2	3.3
Lu	1.12	1.07	1.00	.98	.28	.79	.72	.53	.73	.60	.50	.48	.48
Hf	16.6	16.1	16.4	16.8	11.9	13.1	13.7	12.8	11.5	11.1	10.7	11.6	10.6
Ta	3.7	3.6	3.6	3.3	2.9	3.1	2.9	2.8	2.7	2.5	2.5	2.3	2.4
Pb	36	30	26	12.1	13.4	14.3	30	23	22	16.4	16.8	23	17.4
Th	24	23	23	22	13.5	19.2	17.4	14.8	17.3	15.0	15.5	15.8	14.3
U	6.1	6.1	4.5	7.1	3.1	3.9	3.8	3.7	3.5	3.4	3.2	3.9	3.3
Nb/La	.63	.75	.61	1.22	1.84	1.00	1.08	1.30	.83	1.43	1.21	1.29	1.02
Eu/Eu*[d]	.04	.04	.04	.04	.03	.01	.01	.01	.04	.02	.02	.01	.02
$(La/Sm)_N$	4.7	4.2	4.4	2.6	2.1	3.1	3.1	2.9	3.3	2.9	3.3	3.7	3.1
$(La/Yb)_N$	8.3	8.5	9.2	4.8	9.0	5.9	5.6	5.8	6.1	4.6	5.8	5.8	7.6

Note. LOI = loss on ignition; N = normalized to chondrite (Boynton 1984).
[a] Total Fe as Fe_2O_3.
[b] Mg# = 100 × molar $Mg^{2+}/(Mg^{2+} + TFe^{2+})$.
[c] Data in bold were determined by method of isotope dilution.
[d] $Eu/Eu^* = Eu_N/(Sm_N \times Gd_N)^{0.5}$.

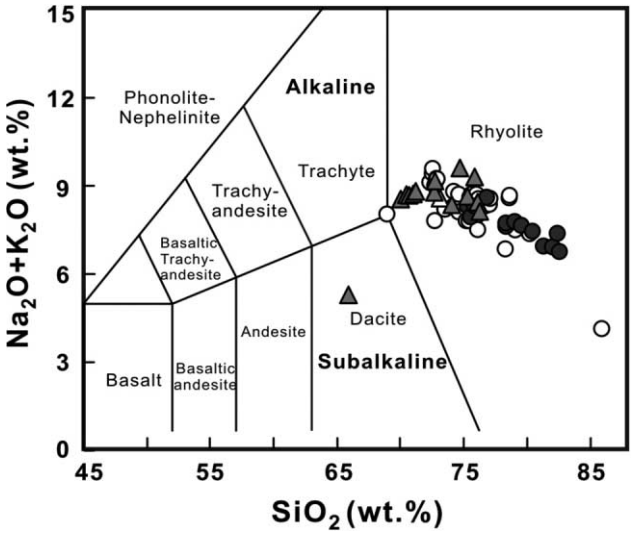

Figure 5. SiO_2 versus Na_2O+K_2O diagram for late Mesozoic felsic volcanic rocks from the Songliao basin. Gray triangles = I-type felsic volcanic rocks; black circles = A-type rhyolites (see fig. 6 for felsite classification). White triangles and circles are data from Meng et al. (2010, 2013) and Zhang et al. (2011). A color version of this figure is available online.

TiO_2, and MgO concentrations compared to the I-type dacites and rhyolites, indicating that the two rock types were formed from different sources and by different magmatic processes.

The total REE contents in the I-type dacites and rhyolites vary from 98 to 217 ppm (average 158 ppm), whereas the A-type rhyolites have slightly higher REE concentrations ranging from 138 to 397 ppm (average 234 ppm). I-type rocks show subparallel REE patterns with slightly fractionated LREE and fractionated, concave HREE patterns (fig. 8*a*). The latter feature can be explained by the presence of amphibole, which occurs as microphenocryst in these rocks. Plagioclase fractionation is indicated by variable Eu anomalies. The A-type rhyolites have uniform REE patterns with concave HREE patterns but show distinct negative Eu anomalies and lower $(La/Yb)_N$ ratios (5–9) compared to the I-type rocks (5–14; fig. 8*c*; tables 1, 2). All felsic rocks have well-defined negative Sr and Eu anomalies (fig. 8*b*, 8*d*) due to extensive feldspar crystallization and negative P anomalies (fig. 8*b*, 8*d*), indicating apatite fractionation during magmatic processes. The negative Ti anomalies (fig. 8*b*, 8*d*) are probably due to fractionation of sphene, and this mineral is also present in thin section. It is noteworthy that the A-type rhyolites are highly depleted in Ba. Their Sr, P, Eu, and Ti anomalies are more pronounced than in the I-type rocks. I-type dacites and rhyolites show negative Nb anomalies compared to the A-type rhyolite samples in which Nb anomalies vary from slightly negative to positive (fig. 8*b*, 8*d*).

The trace elemental concentrations of analyzed zircons are given in table S2. In granitic melts, zircon is one of the early-crystallizing mineral phases, so the composition of zircon reflects the characteristics of primary magma. In the chondrite-normalized REE diagram (fig. 9*b*), all zircons from I- and A-type volcanic rocks show steep positive patterns with negative Eu anomalies and positive Ce anomalies, and these are typical features of zircons from igneous rocks (Hoskin and Schaltegger

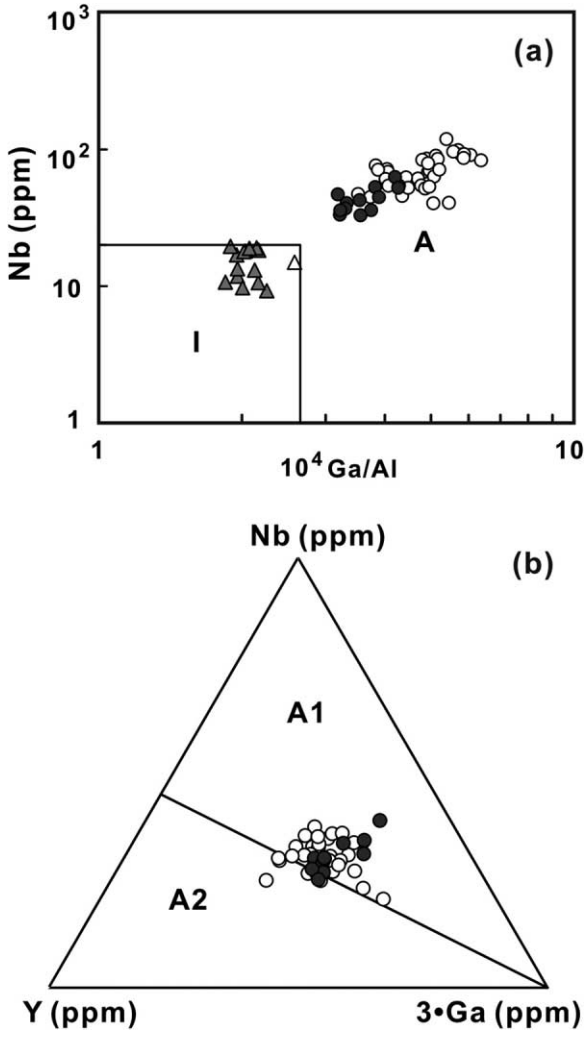

Figure 6. *a*, Ga/Al ratios versus Nb diagram (from Whalen et al. 1987). *b*, A1 and A2 subgroup discriminations of A-type rhyolites in the Songliao basin according to Eby (1992). Symbols as in figure 5. A color version of this figure is available online.

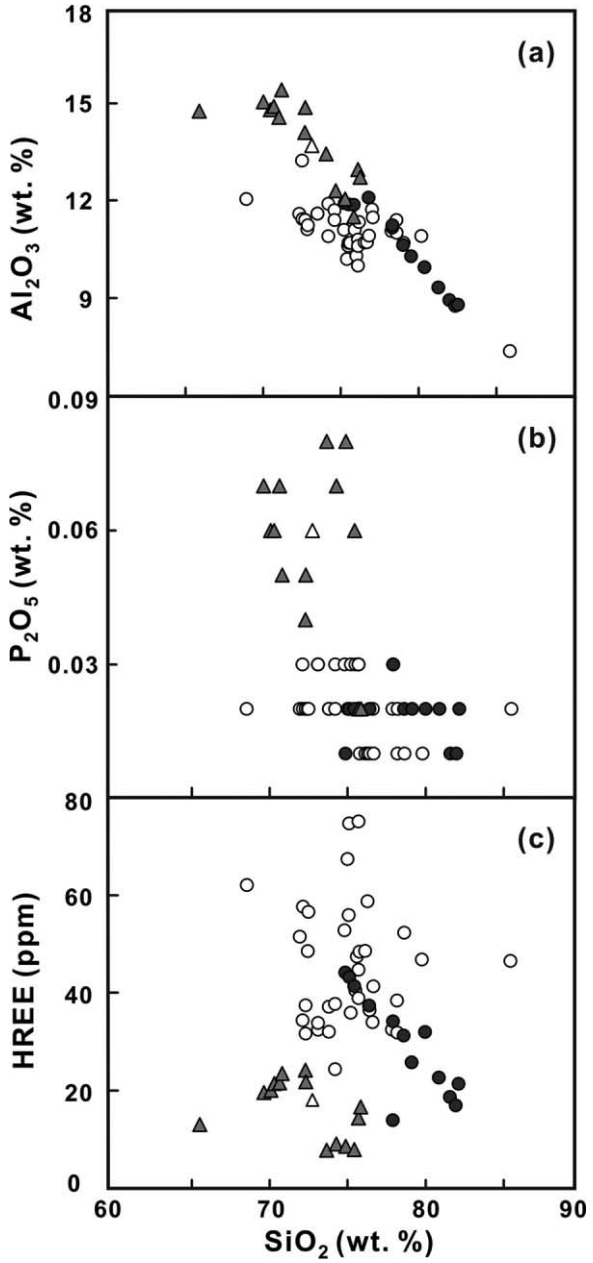

Figure 7. Harker variation diagrams for late Mesozoic A- and I-type dacites and rhyolites from the Songliao region. For a given degree of magma fractionation, the two types of felsic rocks have different elemental concentrations. Symbols as in figure 5. A color version of this figure is available online.

2003). The fractionated LREE pattern, however, could also result from mineral inclusions in zircons. Zircons from the A-type rhyolite sample have higher concentration of HREE (fig. 9*b*) and HFSE (fig. 9*a*), consistent with zircon grains from typical A-type granites, particularly those from anorogenic settings (Nardi et al. 2013). Zircons from A-type rhyolites show pronounced Eu anomalies, indicating that plagioclase fractionation was more important as in the I-type melt (fig. 9*b*).

Whole-Rock Sm-Nd and Zircon Hf Isotopes. Sm-Nd isotope analyses were performed on 15 felsic samples, and the results are presented in table 3 and plotted in figure 11*b*, 11*c*. All samples show relatively homogeneous Nd isotopic compositions. $\varepsilon_{Nd(t)}$ values of I-type dacites/rhyolites (1.2–2.1) and A-type rhyolites (1.9–2.4) are consistent with a derivation from the mantle. All samples have similar Nd model ages, $T_{DM}Nd$, between 0.5 and 0.8 Ga (table 3).

The Hf isotopic composition of zircons provides further information on the source and age of the magmatic protolith. Hf isotopic analyses were performed on the same zircon grains used for U-Pb dating analyses. In situ Hf isotopic analyses of zircons are listed in table S3 and shown in figure 11*a*.

Zircons from I-type felsic rocks have $^{176}Hf/^{177}Hf$ ratios between 0.282876 and 0.283010 and $\varepsilon_{Hf}(t)$ values, when calculated back to 110 Ma, between +5.7 and +10.4. Depleted-mantle model ages, T_{DM} (Hf), are mainly between 540 to 344 Ma (table S3; fig. 11*a*). Zircons in A-type rhyolites show similar $^{176}Hf/^{177}Hf$ ratios (0.282862–0.283021) and $\varepsilon_{Hf}(t)$ values between +5.0 and +11.1. Hf model ages, T_{DM} (Hf), of these zircons vary from 597 to 353 Ma (table S3; fig. 11*a*).

Discussion

Petrogenesis of the Early Cretaceous Volcanic Rocks. Differentiated felsic volcanic rocks are usually generated during long-term magma evolution. Large-volume rhyolite provinces occur in a variety of tectonic settings, including continental margins and continental rift zones (Riley et al. 2001). The petrogenesis of these rocks is important to better understand igneous processes within the continental crust and to constrain the nature of the interaction between continental crust and the underlying mantle (Annen et al. 2006). Two different models are employed to explain the generation of silicic magmas. In the first model, these rocks are related to a mantle-derived parent magma that experienced a high degree of fractional crystallization or assimilation and fractional crystallization. This process is often suggested for small felsic magma batches, because unreasonably large amounts of basalt should be crystallized, to generate large volumes of silicic magma (Shinjo and Kato 2000). The second model, in which basaltic magmas provide heat for the partial melting of crustal rocks, is considered more appropriate for the large-volume rhyolitic eruptions with a general

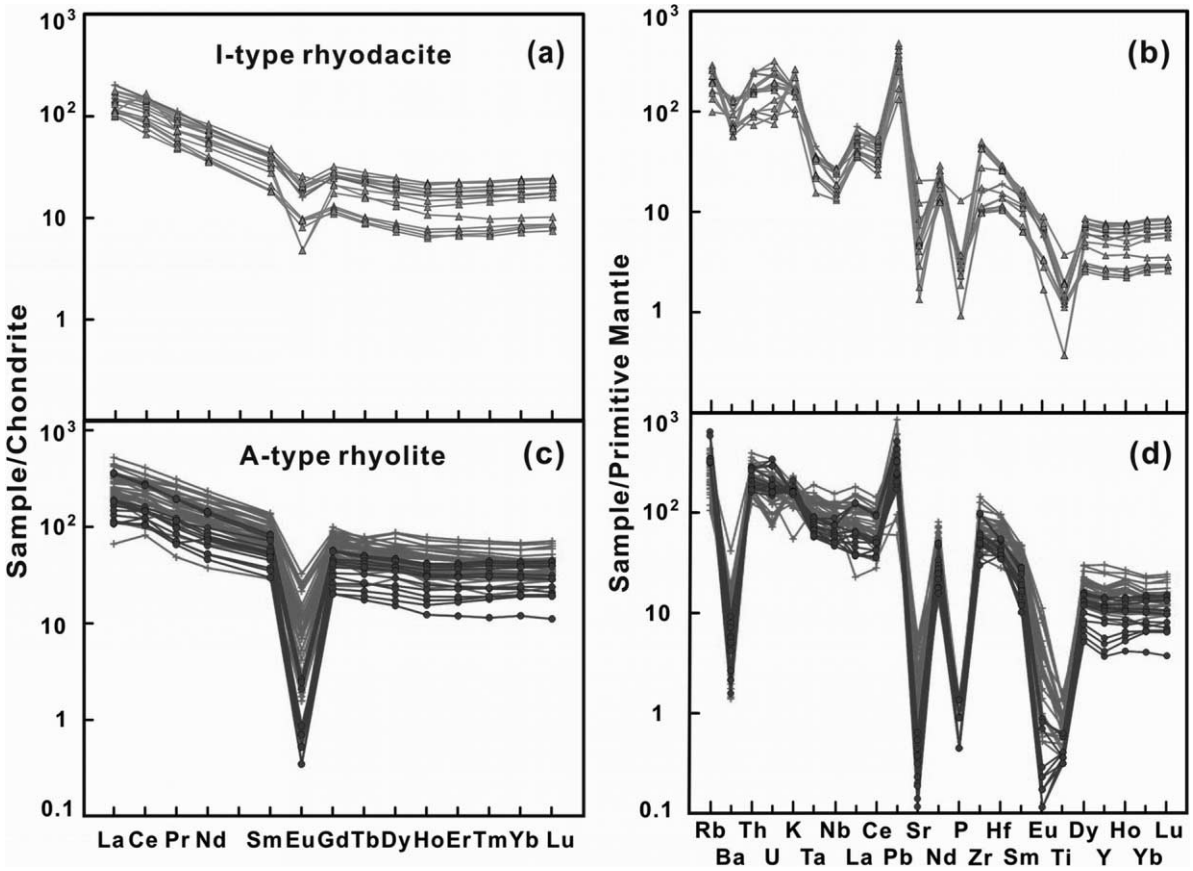

Figure 8. Chondrite-normalized rare earth element patterns and primitive mantle–normalized trace element patterns for I- and A-type dacites and rhyolites from the Songliao basin. Chondrite values are from Boynton (1984) and primitive mantle values from Sun and McDonough (1989). A color version of this figure is available online.

paucity of intermediate products (Bryan et al. 2002; Yamamoto 2007).

The early Cretaceous stratigraphy of the Songliao basin is dominated by rhyolitic rocks interbedded with minor mafic-intermediate lava flows. It has been argued that the volcanic rocks of the Songliao basin were generated in a subduction zone environment (e.g., Wang et al. 2002*a*; Xu et al. 2013). Although the I-type dacites and rhyolites and A-type rhyolites investigated in this study have much in common on geochemical compositions (figs. 5, 8), the representative difference between them (figs. 7, 9, 10) could provide more information on petrogenesis of the felsic rocks. I-type rocks are enriched in large ion lithophile elements (LILEs) and LREE and depleted in HFSE, especially in Nb and Ta (fig. 8*a*, 8*b*), possessing features similar to subduction-related arc rocks that were modified in crustal magma chambers. Zircons in these rocks show depleted Hf-isotope compositions and young Hf and Nd model ages (tables 3, S3; fig. 11*a*), and this excludes the contribution of old crustal material during the genesis of the felsic rocks. Their Nd isotopic ratios plot between the CAOB basement and the depleted mantle, indicating that the involvement of a mantle component, as was already claimed for the subordinate mafic-intermediate volcanic rocks in this area (Wang et al. 2006*b*; Zhang et al. 2009; Song et al. 2010; fig. 11*b*, 11*c*). The origin of these basic rocks, which are isotopically identical to the dacites and rhyolites and also show HFSE depletion and LILE enrichment, has been explained by melting of subduction-modified mantle sources (e.g., Song et al. 2010). The I-type felsic rocks have high Ba/Nb ratios (fig. 10*a*), a diagnostic feature of fluid metasomatism (Gill 1981). In the Pearce diagrams (Pearce et al. 1984; fig. 10*b*, 10*c*), they plot into the volcanic arc field, indicating that their parental magmas have subduction-related affinities. From the arguments outlined above we conclude that the I-type felsic rocks of the Songliao basin formed by partial melting of newly produced crust, which, in turn, was created from subduction-modified mantle material above a subduction zone.

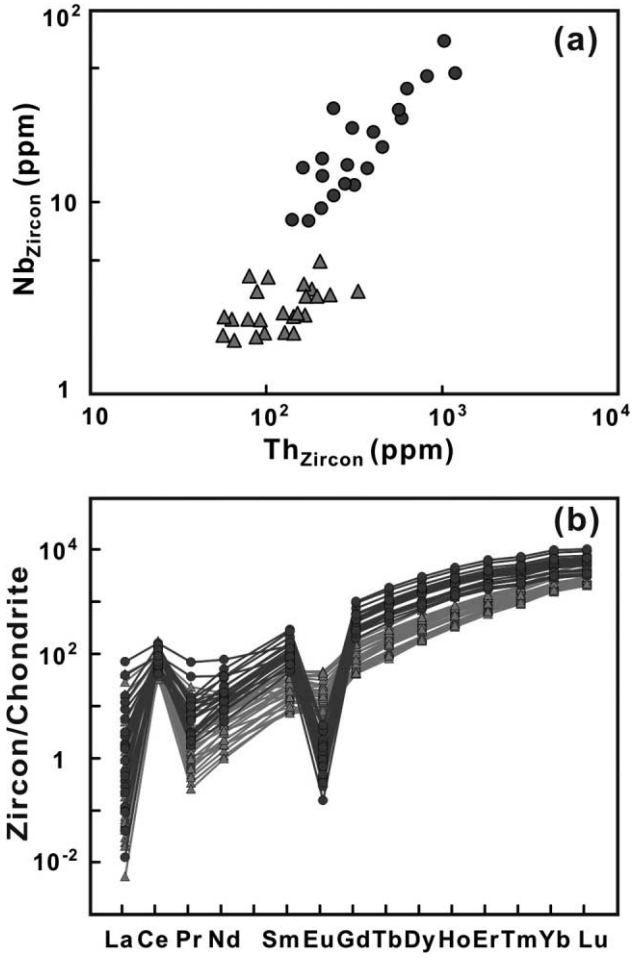

Figure 9. Trace-element data for zircons of late Mesozoic felsic volcanic rocks from the Songliao region. *a*, Th versus Nb diagram for zircons for A- and I-type rhyolites. *b*, Chondrite-normalized rare earth element diagram for zircons for A- and I-type dacites and rhyolites. Chondrite values are from Boynton (1984). Symbols as in figure 2. A color version of this figure is available online.

The I- and A-type felsic rocks have similar trace element patterns, but the latter have more pronounced negative Ba, Sr, P, Eu, and Ti anomalies and higher HFSE and HREE contents, and most A-type samples have no negative Nb-Ta anomalies (fig. 8*d*), which is a general feature of A-type granitoids (La/Nb <1; Martin et al. 1994). A few samples also have high La/Nb ratios, but this is due to the enrichment of REE rather than to the depletion of HFSE such as Nb and Ta (tables 1, 2).

Although A-type granites are usually associated with extensional tectonic environments, there is no clear consensus on their origin. Models of formation range from fractionation of basaltic magmas, with or without crustal contamination (e.g., Loiselle and Wones 1979; Turner et al. 1992; Smith et al. 1999; Anderson and Morrison 2005), to melting of deep crustal lithologies such as granulitic metaigneous rocks that were previously depleted by extraction of a hydrous felsic melt (e.g., Collins et al. 1982; Clemens et al. 1986; Whalen et al. 1987). Experimental and geochemical investigations indicate that A-type granites form at higher temperatures than calc-alkaline rocks (Clemens et al. 1986; King et al. 2001). This suggests that extensive fractional crystallization of mantle-derived intermediate and mafic magma does not play a major role during the formation of A-type granites. Besides, large volumes of mafic to intermediate rocks, as would be expected if extensive fractional crystallization took place, are usually absent (Sylvester 1989). In addition, the rhyolites that lack Nb and Ta anomalies cannot be generated from mafic or intermediate melts by fractional crystallization since this process would cause strong depletion of Nb and Ta.

Because the A-type rhyolites are closely associated with I-type dacites and rhyolites in the Songliao basin, it is unlikely that their parental magma was derived from the depleted mantle. All volcanic rocks of the Songliao basin have similar isotopic composition, and this signature gives rise to the assumption that they were derived from the same source. It has been proposed that A-type granites can originate from partial melting of F- and/or Cl-enriched dry, granulitic (or charnockitic) residue from which a granitoid melt was previously extracted (Collins et al. 1982; Clemens et al. 1986; Landenberger and Collins 1996; King et al. 1997). A similar origin has been discussed for rhyolites around the Hailar basin, about 600 km northwest of the Songliao basin (Li et al. 2014*a*). These authors argue that the A-type rhyolites, which formed after a long period of I-type magma production, were generated by high-temperature partial melting of lower continental crust, which was depleted by previous I-type melt extraction, and the anhydrous melting with high F contents increased the HFSE contents in the melt (Li et al. 2014*a*). Considering a similar geological background (fig. 1*a*), we advocate the conclusion that the A-type rhyolites in Songliao basin were generated by similar processes.

Although I- and A-type felsic rocks show consistent isotopic compositions (fig. 11), they probably had different protoliths. This is supported by the differences in trace-element patterns discussed before. The zircons of the two types of felsic rock also show distinct compositional features. Zircon was an early-crystallizing mineral in both I- and A-type rhyolitic rocks and became included in bio-

Table 3. Sm-Nd Isotopic Data for Late Mesozoic Felsic Volcanic Rocks from Songliao Basin

Sample	Sm [ppm]	Nd [ppm]	$^{147}Sm/^{144}Nd$ (m.)	$^{143}Nd/^{144}Nd$ (m.)	$\pm 2\sigma_m$	T_{DM}[a] [Ma]	$\varepsilon_{Nd(t)}$
I-type felsic rocks:							
FK11-125	5.14	28.02	.1109	.512633	.000011	615	1.2
FK11-118	6.40	34.42	.1124	.512636	.000013	619	1.3
FK11-120	6.47	34.98	.1117	.512654	.000011	589	1.6
FK11-114	6.23	32.11	.1173	.512652	.000010	625	1.5
FK11-115	7.33	39.25	.1129	.512656	.000010	592	1.7
SL0917	2.86	17.67	.0978	.512664	.000013	507	2.0
FK11-110	2.80	17.13	.0988	.512656	.000012	522	1.9
FK11-124	4.28	22.99	.1126	.512680	.000010	556	2.1
A-type rhyolites:							
SL0902	4.53	21.26	.1287	.512691	.000015	638	2.1
SL0933	10.9	45.22	.1459	.512691	.000013	793	1.9
FK11-93	11.6	63.03	.1113	.512689	.000013	536	2.3
FK11-139	7.81	34.84	.1355	.512684	.000011	704	1.9
FK11-140	9.23	40.39	.1381	.512703	.000009	690	2.2
FK11-135	8.11	35.68	.1375	.512710	.000010	672	2.4
FK11-104	8.39	37.31	.1359	.512706	.000010	666	2.3

Notes. Initial $\varepsilon_{Nd(t)}$ was calculated for 110 Ma, the emplacement age of the felsic rocks of this study, with the parameter of Bouvier et al. (2008). m. = measured isotopic ratio.
[a] Model age calculation according to DePaolo (1981).

tite, magnetite, and feldspars during subsequent crystallization according to the observation of thin sections. Zircons in A-type rhyolites have extremely negative Eu anomalies and higher HFSE and HREE concentrations than zircons from I-type felsic rocks (fig. 9). It is also noticeable in figure 10*a* that the A-type felsic rocks have low Ba/Nb and high Nb/La ratios and plot in the field of within-plate granitoids in the Pearce diagrams (fig. 10*b*, 10*c*). Together with their A1 affinities (Eby 1992; fig. 6*b*), we suggest that the parental magma of the A-type rhyolites was generated under anhydrous conditions and at considerable high temperatures. It seems most likely that Mesozoic extension of the lithosphere beneath NE China led to melting of juvenile lower crust and the production of A-type rhyolites.

Age Constraints on Lithospheric Extension. It has been previously suggested that volcanism in the Songliao basin lasted from 160 to 102 Ma, with two major peaks in the late Jurassic (157–147 Ma) and early Cretaceous (139–113 Ma), corresponding to the Huoshiling and Yingcheng volcanic episodes, respectively (Wang et al. 2002*a*, 2002*b*). Recently performed high-precision age determinations, however, show evidence for younger (i.e., early Cretaceous) ages of volcanic rocks from the Huoshiling (133–129 Ma; Pei et al. 2008) and Yingcheng (120–109 Ma; Ding et al. 2007; Jin et al. 2011; Zhang et al. 2011) Formations.

The Yingcheng Formation hosts the most widespread volcanic rocks within the Songliao basin. The zircons from I- and A-type volcanic rocks of this formation show identical U-Pb ages of 114 ± 2 and 113 ± 2 Ma (fig. 4). These results are consistent with previously obtained U-Pb zircon ages from volcanic rocks of the Yingcheng Formation. Our samples were collected from the uppermost section of the Yingcheng Formation and, therefore, it can be assumed that the zircon ages date the final stage of intense volcanic activity within the Songliao basin.

Geophysical data indicate a present-day crustal thickness of about 30 km below the Songliao basin, and this crust is underlain by ca. 30–50 km of mantle lithosphere (Xu et al. 2000; An and Shi 2006; Li et al. 2006). The Moho depth varies from 27 to 36 km, with the shallowest and deepest parts being located at the eastern and northwest flanks of the basin, respectively (Tao et al. 2014). The Songliao basin experienced intense rifting and extension during late Mesozoic lithospheric thinning in NE China (e.g., Meng 2003). Thickness estimates for the early Cretaceous amount to ~28 km for the crust and ~30 km for the underlying lithospheric mantle (Xu et al. 2000).

The bulk composition of the rocks together with inferences about the residues left from melting can be used to evaluate the petrogenesis of the volcanic rocks. Adakitic rocks have high Sr values, high La/Yb and Sr/Y ratios, low HREE and Y contents, and no significant Eu anomalies. These characteristics imply that the equilibrated residues were garnet rich and that plagioclase was not a significant residual phase (Nash and Crecraft 1985; Otamendi

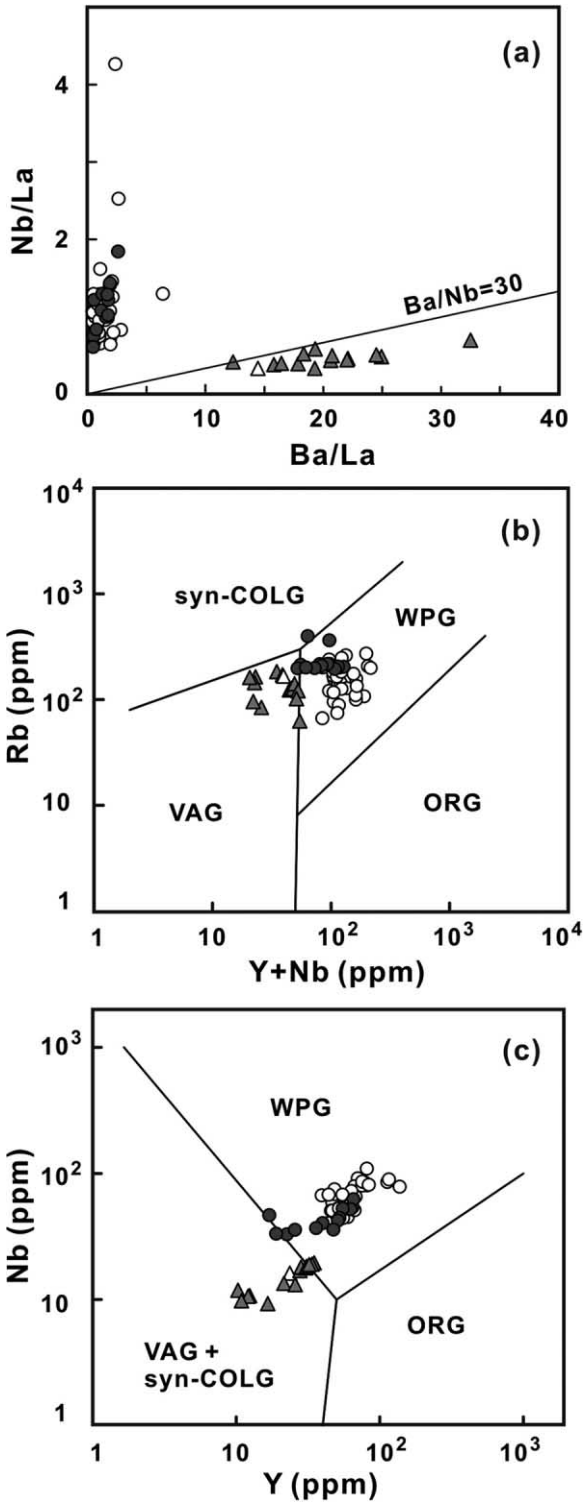

Figure 10. *a*, Ba/La versus Nb/La ratios for A- and I-type felsic volcanic rocks from the Songliao basin. Ba/Nb ratios >30 indicate subduction-related magmas (Gill 1981). *b*, *c*, Tectonic discrimination diagrams for the late Mesozoic felsic volcanic rocks of the Songliao region (after Pearce et al. 1984). WPG = within-plate granite; ORG = ocean ridge granite; VAG = volcanic arc granite; syn-COLG = syncollision granite. Symbols as in figure 5. A color version of this figure is available online.

et al. 2002). It has been suggested that the Sr and Yb contents of intermediate to felsic magmatic rocks, if controlled by residual phases, provide information about the pressure during magma generation (Zhang et al. 2006*a*, 2006*b*; Zhang and Li 2012). The I- and A-type rocks from the Songliao basin have geochemical features in common with the Zhemin-type (Sr between 40 and 400 ppm, Yb >1.5 ppm, Al_2O_3 between 12% and 17%, Eu/Eu^* from 0.4 to 1.0) and Nanling-type (Sr <100 ppm, Yb >1.5 ppm, Al_2O_3 <14%, Eu/Eu^* often under 0.4) granite according to Zhang et al. (2006*a*, 2006*b*) and Zhang and Li (2012). The negative Sr and Eu anomalies of the A-type rhyolites, together with low MgO, CaO, P_2O_5, Al_2O_3, and TiO_2 content and high K_2O content (fig. 8*c*, 8*d*; tables 1, 2), imply that these rocks were in equilibrium with a plagioclase-, hornblende-, and pyroxene-rich residue. In such case, resulting liquids are low in Al_2O_3, which is retained in the source by residual plagioclase, and FeO_t cannot be effectively retained by Mg-rich pyroxenes and amphiboles (Hollocher et al. 2002). Such residue can form only at pressures <10 kbar (Wolf and Wyllie 1994; Springer and Seck 1997; Zhang and Li 2012).

The I-type dacites and rhyolites of the Songliao basin have higher Sr and Al_2O_3 concentrations compared to their A-type counterparts (tables 1, 2). In the I-type rocks moderate negative Eu anomalies are present only in whole-rock data (fig. 8*a*, 8*b*), not in zircon data (fig. 9*b*). This implies that residual plagioclase was less important in their petrogenesis. Whereas I-type melts can be produced in continental crust far exceeding normal crustal thickness, A-type rhyolites, with extremely low Sr values and negative Eu anomalies, are related to crustal source regions less than 30 km (Zhang et al. 2006*a*, 2006*b*; Zhang and Li 2012). Based on these observations it is suggested that the A-type rhyolites of the Songliao basin were produced by lithospheric thinning during extension. During this phase, upwelling asthenosphere provided sufficient heat for crustal melting. Based on the age of these A-type rhyolites, this lithospheric thinning occurred around 110 Ma.

Tectonic Implications. It is generally assumed that the Songliao basin and adjacent areas were subjected to extensional tectonics during the late Mesozoic (Shao et al. 2001; Fan et al. 2003; Gao et al. 2005; Wu et al. 2005). Crustal extension during the Cretaceous was widespread in NE Asia, and this is evident from

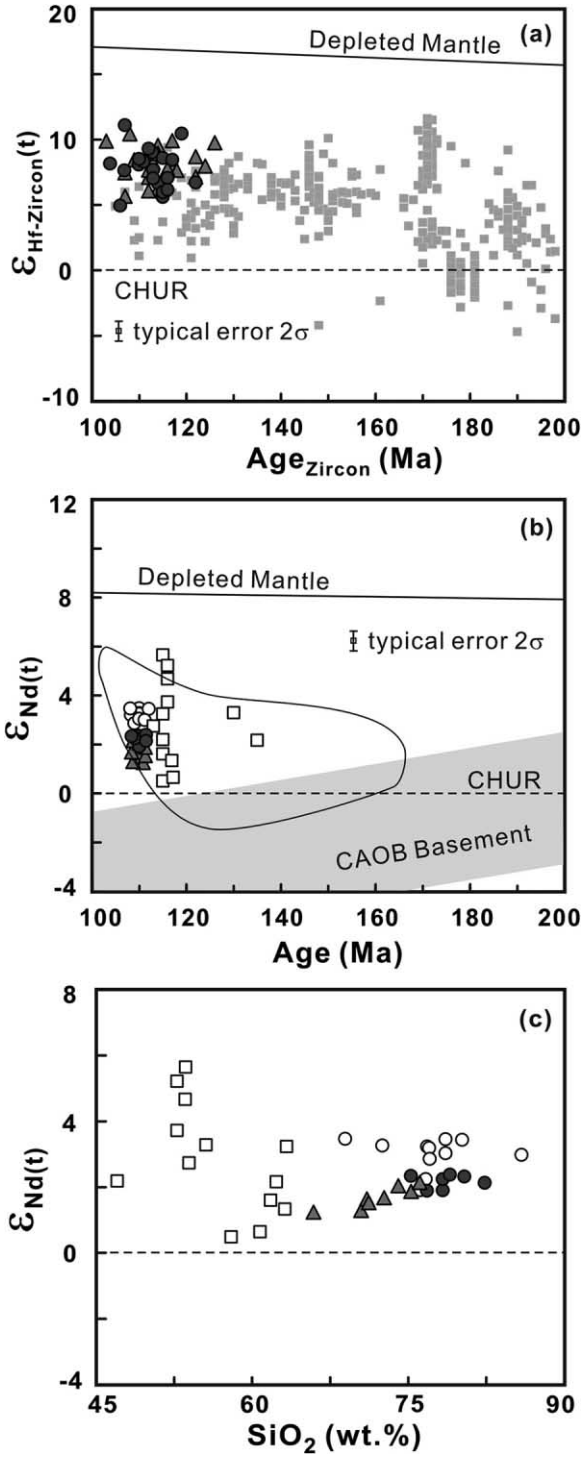

Figure 11. *a*, Zircon Hf isotopic evolution diagram for A- and I-type rhyolites from the Songliao region. Gray squares represent data for Mesozoic granitic rocks in NE China (Sui et al. 2007; Wu et al. 2011*b*; Zeng et al. 2011; Zhou et al. 2013; Li et al. 2014*b*). *b*, Nd isotopic evolution diagram for late Mesozoic volcanic rocks from the Songliao basin. Initial ε_{Nd} values (t = 110 Ma) are plotted as a group for better visibility of data points. Open squares = data from mantle-derived samples (Wang et al. 2006*b*; Zhang et al. 2009; Song et al. 2010). Data field: solid line = Mesozoic granitic rocks from the Songliao basin (Wu et al. 2000, 2001, 2003); field in gray = middle Carboniferous to middle Permian Central Asian Orogenic Belt basement (data from Wu et al. 2000; Jian et al. 2008; Chen et al. 2009). *c*, SiO_2 versus initial ε_{Nd} values showing isotopic similarity between mantle- and crust-derived felsic volcanic rocks. Symbols as in figures 2, 5. A color version of this figure is available online.

the presence of extensive rift basins (e.g., Ren et al. 2002; Meng 2003; Wang et al. 2011), widespread calc-alkaline magmatism (e.g., Fan et al. 2003; Tomurtogoo et al. 2005), and metamorphic core complexes (e.g., Wang et al. 2011). Mylonites from core complexes in NE Asia yield $^{40}Ar/^{39}Ar$ cooling ages of 130–110 Ma (Wang et al. 2011) identical to the ages of A-type granites and volcanic rocks in NE China (Wu et al. 2002, 2005; this study). However, the mechanism of crust extension of NE China during this period is still a matter of debate because of superposed events such as Paleo-Asian ocean closure and circum-Pacific and Mongol-Okhotsk tectonic regimes.

Large-scale extension and widespread Mesozoic volcanic eruption in NE China have been explained by upwelling mantle plume (Ge et al. 1999; Lin et al. 2000; Dobretsov and Vernikovsky 2001), postorogenic collapse of overthickened lithosphere after closure of the Mongol-Okhotsk Ocean (Fan et al. 2003; Meng 2003; Wang et al. 2006*a*), back-arc lithospheric extension due to rollback of the subducting Paleo-Pacific plate (Zhao et al. 1989; Faure and Natalin 1992; Li and Shu 2002; Sun et al. 2013), and lithospheric delamination (Tomurtugoo et al. 2005; Wu et al. 2005; Wang et al. 2006*a*; Zhang et al. 2010). Several models (e.g., Wang et al. 2006*a*; Zhang et al. 2010, 2011) rest on the observation that the age of the volcanic rocks decreases from west to east, but this age migration is still a controversial subject as the igneous rocks were generated under a complex geological context between the Paleo-Asian Ocean and the Mongol-Okhotsk and circum-Pacific tectonic regimes (Xu et al. 2013). For example, for contemporaneous magmatic activity in western Great Xing'an and eastern Zhangguangcai (mafic intrusions and porphyry Cu-Mo deposit both emplaced at 180–170 Ma), different geodynamic settings were proposed (Zhang et al. 2010; Chen et al. 2011; Yu et al. 2012; Zhou et al. 2013). Moreover, new zircon U-Pb ages of the volcanic rocks are much younger than the previous Ar-Ar and Rb-Sr dating results. Therefore, it is necessary to reeval-

uate the timing of the Mesozoic volcanic activity in NE China.

Volcanic rocks of the Hailar basin, Great Xing'an range, have many features in common with the I- and A-type dacites/rhyolites investigated in this study. In the Hailar basin, long-lasting I-type volcanic activity was followed by eruptions of A-type rhyolites (Li et al. 2014*a*). The A-type rhyolites in both basins have identical geochemical characteristics and show a young trend from Hailar to Songliao from 125 to 110 Ma. This signature could imply that Mesozoic lithospheric extension ceased asynchronously from west to east. Moreover, this migration could be related to the rollback process of the Paleo-Pacific subducted plate (e.g., Wu et al. 2005; Zhang et al. 2010), which led to asthenosphere uprising from Hailar in the west to Songliao in the east.

Conclusions

I- and A- type dacites and rhyolites were identified in the early Cretaceous Yingcheng Formation of the Songliao basin. Whole-rock and zircon geochemical characteristics of these rocks confirm their derivation from different protoliths. I-type rocks were generated by partial melting of newly formed crust that originated from partial melting of subduction-modified mantle sources. Geochemical features of the A-type rhyolites support partial melting of I-type felsic lower crust under anhydrous conditions at considerable high temperatures during a period of lithosphere extension.

Zircons of the A- and I-type volcanic rocks show identical U-Pb ages of ~110 Ma. Geochemical features of the A-type rhyolites (low Sr, Al_2O_3, strongly negative Eu anomalies in whole rock and zircon, high contents of HREE and HFSE) reflect a shallow crustal melting depth. We conclude that the amount of thinning of the lithosphere below the Songliao basin reached its maximum around 110 Ma.

Mesozoic lithospheric extension in NE China ceased asynchronously from west to east from 125 to 110 Ma. This migration might be related to the rollback process of the Paleo-Pacific subducted plate.

ACKNOWLEDGMENTS

This study was financially supported by the Ministry of Science and Technology of China (grant 2009CB219305) and the National Nature Science Foundation of China (grants 41372072 and 41090372). E. Hegner and J. F. He are thanked for help during isotopic analyses.

REFERENCES CITED

An, M., and Shi, Y. 2006. Lithospheric thickness of the Chinese continent. Phys. Earth Planet. Inter. 159:257–266.

Andersen, T. 2002. Correction of common lead in U-Pb analyses that do not report ^{204}Pb. Chem. Geol. 192:59–79.

Anderson, J. L., and Morrison, J. 2005. Ilmenite, magnetite, and peraluminous Mesoproterozoic anorogenic granites of Laurentia and Baltica. Lithos 80:45–60.

Annen, C.; Blundy, J. D.; and Sparks, R. S. J. 2006. The genesis of intermediate and silicic magmas in deep crustal hot zones. J. Petrol. 47:505–539.

Bouvier, A.; Vervoort, J. D.; and Patchett, P. J. 2008. The Lu-Hf and Sm-Nd isotopic composition of CHUR: constraints from unequilibrated chondrites and implications for the bulk composition of terrestrial planets. Earth Planet. Sci. Lett. 273:48–57.

Boynton, W. V. 1984. Geochemistry of the rare earth elements: meteorite studies. *In* Henderson, P., ed. Rare earth element geochemistry. Amsterdam, Elsevier, p. 63–114.

Bryan, S. E.; Riley, T. R.; Jerram, D. A.; Stephens, C. J.; and Leat, P. T. 2002. Silicic volcanism: an undervalued component of large igneous provinces and volcanic rifted margins. *In* Menzies, M. A.; Klemperer, S. L.; Ebinger, C. J.; and Baker, J., eds. Volcanic rifted margins. Geol. Soc. Am. Spec. Pap. 362:99–120.

Chen, B.; Jahn, B. M.; and Tian, W. 2009. Evolution of the Solonker suture zone: constraints from zircon U-Pb ages, Hf isotopic ratios and whole-rock Nd-Sr isotopic compositions of subduction- and collision-related magmas and forearc sediments. J. Asian Earth Sci. 34:245–257.

Chen, Z.; Zhang, L.; Wan, B.; Wu, H.; and Cleven, N. 2011. Geochronology and geochemistry of the Wunugetushan porphyry Cu-Mo deposit in NE China, and their geological significance. Ore Geol. Rev. 43:92–105.

Clemens, J. D.; Holloway, J. R.; and White, A. J. R. 1986. Origin of an A-type granite: experimental constraints. Am. Mineral. 71:317–324.

Collins, W. J.; Beams, S. D.; White, A. J. R.; and Chappell, B. W. 1982. Nature and origin of A-type granites with particular reference to southeastern Australia. Contrib. Mineral. Petrol. 80:189–200.

DePaolo, D. J. 1981. A neodymium and strontium isotopic study of the Mesozoic calc-alkaline granitic batholiths of the Sierra-Nevada and Peninsular Ranges, California. J. Geophys. Res. 86:470–488.

Ding, R. X.; Shu, P.; Ji, X. Y.; Qu, Y. M.; Cheng, R. H.; and Zhang, B. 2007. SHRIMP zircon U-Pb age and geological meaning of reservoir volcanic rocks in Qingshen gas field of the Songliao basin, NE China. J. Jilin Univ. 3:525–530 (in Chinese with English abstract).

Dobretsov, N. L.; Berzin, N. A.; and Buslov, M. M. 1995. Opening and tectonic evolution of the Paleo-Asian Ocean. Int. Geol. Rev. 37:335–360.

Dobretsov, N. L., and Vernikovsky, V. A. 2001. Mantle plumes and their geologic manifestations. Int. Geol. Rev. 43:771–787.

Eby, G. N. 1992. Chemical subdivision of the A-type granitoids: petrogenetic and tectonic implications. Geology 20:641–644.

Fan, W. M.; Guo, F.; Wang, Y. J.; and Lin, G. 2003. Late Mesozoic calc-alkaline volcanism of post-orogenic extension in the northern Da Hinggan Mountains, northeastern China. J. Volcanol. Geotherm. Res. 121: 115–135.

Faure, M., and Natalin, B. 1992. The geodynamic evolution of the eastern Eurasian margin in Mesozoic times. Tectonophysics 208:397–411.

Gao, X. F.; Guo, F.; Fan, W. M.; Li, C. W.; and Li, X. Y. 2005. Origin of late Mesozoic intermediate-felsic volcanic rocks from the northern Da Hinggan Mountains, NE China. Acta Petrol. Sin. 21:737–748 (in Chinese with English abstract).

Ge, R.; Zhang, Q.; Wang, L.; Chen, J.; Xie, G.; and Wang, X. 2012. Late Mesozoic rift evolution and crustal extension in the central Songliao Basin, northeastern China: constraints from cross-section restoration and implications for lithospheric thinning. Int. Geol. Rev. 54:183–207.

Ge, W. C.; Lin, Q.; Sun, D. Y.; Wu, F. Y.; Won, C. K.; Lee, M. W.; Jin, M. S.; and Yun, S. H. 1999. Geochemical characteristics of the Mesozoic basalts in Da Hinggan Ling: evidence of the mantle-crust interaction. Acta Petrol. Sin. 15:397–407 (in Chinese with English abstract).

Gill, J. B. 1981. Orogenic andesites and plate tectonics. New York, Springer.

Graham, S. A.; Cope, T.; Johnson, C. L.; and Ritts, B. 2012. Sedimentary basins of the late Mesozoic extensional domain of China and Mongolia. *In* Roberts, D. G., and Bally, A. W., eds. Phanerozoic rift systems and sedimentary basins. Amsterdam, Elsevier, p. 443–461.

Guo, Z.; Wilson, M.; Liu, J.; and Mao, Q. 2006. Post-collisional, potassic and ultrapotassic magmatism of the northern Tibetan Plateau: constraints on characteristics of the mantle source, geodynamic setting and uplift mechanisms. J. Petrol. 47:1177–1220.

Hanchar, J. M., and Hoskin, P. W. O. 2003. Zircon. Rev. Mineral. Geochem. 53, 500 p.

Hegner, E.; Walter, H. J.; and Satir, M. 1995. Pb-Sr-Nd isotopic compositions and trace element geochemistry of megacrysts and melilitites from the Tertiary Urach volcanic field: source composition of small volume melts under SW Germany. Contrib. Mineral. Petrol. 122:322–335.

Hollocher, K.; Bull, J.; and Robinson, P. 2002. Geochemistry of the metamorphosed Ordovician Taconian Magmatic Arc, Bronson Hill anticlinorium, western New England. Phys. Chem. Earth 27:5–45.

Hoskin, P. W. O., and Schaltegger, U. 2003. The composition of zircon and igneous and metamorphic petrogenesis. Rev. Mineral. Geochem. 53:27–62.

Hou, Z. H., and Wang, C. Z. 2007. Determination of 35 trace elements in geological samples by inductively coupled plasma mass spectrometry. J. Univ. Sci. Technol. China 37:940–944 (in Chinese with English abstract).

Itsikson, M. I.; Krasnyi, L. I.; and Matveenko, V. T. 1965. Circum-Pacific volcanic belts and their metallogeny. Ore Potential Volcan. Form., p. 181–196 (in Russian).

JBGMR (Jilin Bureau of Geology and Mineral Resources). 1988. Regional geology of Jilin Province. Geological Publishing House, Beijing (in Chinese with English summary).

Jian, P.; Liu, D. Y.; Kröner, A.; Windley, B. F.; Shi, Y. R.; Zhang, F. Q.; Shi, G.; et al. 2008. Time scale of an early to mid-Paleozoic orogenic cycle of the long-lived Central Asian Orogenic Belt, Inner Mongolia of China: implications for continental growth. Lithos 101:233–259.

Jin, X.; Ge, W. C.; Xue, Y. F.; and Jin, Y. D. 2011. Zircon U-Pb ages and Hf isotopic composition of volcanic rocks from Well Linshen 3 in Songliao Basin. Glob. Geol. 1:1–17 (in Chinese with English abstract).

Jochum, K. P.; Nohl, U.; Herwig, K.; Lammel, E.; Stoll, B.; and Hofmann, A. W. 2005. GeoReM: a new geochemical database for reference materials and isotopic standards. Geostand. Geoanal. Res. 29:333–338.

King, P. L.; Chappell, B. W.; Allen, C. M.; and White, A. J. R. 2001. Are A-type granites the high-temperature felsic granites? evidence from fractionated granites of the Wangrah Suite. Aust. J. Earth Sci. 48:501–514.

King, P. L.; White, A. J. R.; Chappell, B. W.; and Allen, C. M. 1997. Characterization and origin of aluminous A-type granites from the Lachlan Fold Belt, southeastern Australia. J. Petrol. 38:371–391.

Landenberger, B., and Collins, W. J. 1996. Derivation of A-type granites from a dehydrated charnockitic lower crust: evidence from the Chaelundi complex, eastern Australia. J. Petrol. 37:145–170.

Le Bas, M. J.; Le Maitre, R. W.; Streckeisen, A.; and Zanettin, B. 1986. A chemical classification of volcanic-rocks based on the total alkali silica diagram. J. Petrol. 27:745–750.

Li, J., and Shu, L. S. 2002. Mesozoic-Cenozoic tectonic features and evolution of the Songliao Basin, NE China. J. Nanjing Univ. 38:525–531 (in Chinese with English abstract).

Li, S.; Mooney, W. D.; and Fan, J. 2006. Crustal structure of mainland China from deep seismic sounding data. Tectonophysics 420:239–252.

Li, S. Q.; Chen, F.; Siebel, W.; Wu, J. D.; Zhu, X. Y.; Shan, X. L.; and Sun, X. M. 2012. Late Mesozoic tectonic evolution of the Songliao Basin, NE China: evidence

from detrital zircon ages and Sr-Nd isotopes. Gondwana Res. 22:943–955.

Li, S. Q.; Hegner, E.; Yang, Y. Z.; Wu, J. D.; and Chen, F. 2014*a*. Age constraints on late Mesozoic lithospheric extension and origin of bimodal volcanic rocks from the Hailar basin, NE China. Lithos 190–191:204–219.

Li, S. T.; Mo, X. X.; and Yang, S. G. 1995. Evolution of Circum-Pacific basins and volcanic belts in East China and their geodynamic background. J. China Univ. Geosci. 6:48–58.

Li, Z. Z.; Qin, K. Z.; Li, G. M.; Ishihara, S.; Jin, L. Y.; Song, G. X.; and Meng, Z. J. 2014*b*. Formation of the giant Chalukou porphyry Mo deposit in northern Great Xing'an Range, NE China: partial melting of the juvenile lower crust in intra-plate extensional environment. Lithos 202–203:138–156.

Lin, Q.; Ge, W. C.; Sun, D. Y.; Wu, F. Y.; Won, C. K.; Lee, M. W.; Yun, S. H.; Jin, M. S.; Min, K. D.; and Kwon, C. S. 2000. Genetic relationships between two types of Mesozoic rhyolite and basalts in Great Xingan Ridge. J. Changchun Univ. Sci. Technol. 30:322–328 (in Chinese with English abstract).

Liu, J.; Han, J.; and Fyfe, W. S. 2001. Cenozoic episodic volcanism and continental rifting in northeast China and possible link to Japan Sea development as revealed from K-Ar geochronology. Tectonophysics 339: 385–401.

Liu, X.; Gao, S.; Diwu, C.; Yuan, H.; and Hu, Z. 2007. Simultaneous in-situ determination of U-Pb age and trace elements in zircon by LA-ICP-MS in 20 μm spot size. Chin. Sci. Bull. 52:1257–1264.

Loiselle, M. C., and Wones, D. R. 1979. Characteristics and origin of anorogenic granites. Geol. Soc. Am. Abstr. Program 11:468.

Ludwig, K. R. 2003. ISOPLOT 3: a geochronological toolkit for Microsoft Excel. Berkeley Geochronology Center Special Publication 4. Berkeley, Berkeley Geochronology Center.

Martin, H.; Bonin, B.; Capdevila, R.; Jahn, B. M.; Lameyre, J.; and Wang, Y. 1994. The Kuiqi peralkaline granitic complex (SE China): petrology and geochemistry. J. Petrol. 35:983–1015.

Meng, F. C.; Liu, J. Q.; Li, M.; Liu, X.; Yin, C. H.; Lu, J. M.; and Cui, Y. 2010. Geochemistry and tectonic implications of rhyolites from Yingcheng Formation in Xujiaweizi, Songliao Basin. Acta Petrol. Sin. 26:227–241 (in Chinese with English abstract).

Meng, F. C.; Lu, Y. L.; Liu, J. Q.; and Cui, Y. 2013. Geochemical characteristics and petrogenesis of two types of acid volcanic rocks from Yingcheng Formation in Songliao Basin. Acta Petrol. Sin. 29:2731–2745 (in Chinese with English abstract).

Meng, Q. R. 2003. What drove late Mesozoic extension of the northern China-Mongolia tract? Tectonophysics 369:155–174.

Nardi, L. V. S.; Formoso, M. L. L.; Müller, I. F.; Fontana, E.; Jarvis, K.; and Lamarão, C. 2013. Zircon/rock partition coefficients of REEs, Y, Th, U, Nb, and Ta in granitic rocks: uses for provenance and mineral exploration purposes. Chem. Geol. 335:1–7.

Nash, W. P., and Crecraft, H. R. 1985. Partition coefficients for trace elements in silicic magmas. Geochim. Cosmochim. Acta 49:2309–2322.

Otamendi, J. E.; De La Rosa, J. D.; Douce, A. E. P.; and Castro, A. 2002. Rayleigh fractionation of heavy rare earths and yttrium during metamorphic garnet growth. Geology 30:159–162.

Pearce, J. A.; Harris, N. B. W.; and Tindle, A. G. 1984. Trace-element discrimination diagrams for the tectonic interpretation of granitic rocks. J. Petrol. 25:956–983.

Pei, F. P.; Xu, W. L.; Yang, D. B.; Ji, W. Q.; Yu, Y.; and Zhang, X. Z. 2008. Mesozoic volcanic rocks in the southern Songliao basin: zircon U-Pb ages and their constraints on the nature of basin basement. Earth Sci. 5:603–617 (in Chinese).

Pei, F. P.; Xu, W. L.; Yang, D. B.; Zhao, Q. G.; Liu, X. M.; and Hu, Z. C. 2007. Zircon U-Pb geochronology of basement metamorphic rocks in the Songliao basin. Chin. Sci. Bull. 52:942–948.

Ren, J. Y., and Li, S. T. 1998. Comparison between the faulted basin system in northeastern Asia and the extension of the Basin and Range Province in western North America. Geol. Sci. Technol. Inf. 17:7–11 (in Chinese with English abstract).

Ren, J. Y.; Tamaki, K.; Li, S. T.; and Zhang, J. X. 2002. Late Mesozoic and Cenozoic rifting and its dynamic setting in eastern China and adjacent areas. Tectonophysics 344:175–205.

Riley, T. R.; Leat, P. T.; Pankhurst, R. J.; and Harris, C. 2001. Origins of large volume rhyolitic volcanism in the Antarctic Peninsula and Patagonia by crustal melting. J. Petrol. 42:1043–1065.

Ritts, B. D.; Darby, B. J.; and Cope, T. 2001. Early Jurassic extensional basin formation in the Daqing Shan segment of the Yinshan belt, northern North China Block, Inner Mongolia. Tectonophysics 339:239–258.

Sengör, A. M. C.; Natalin, B. A.; and Burtman, V. S. 1993. Evolution of the Altaid tectonic collage and Paleozoic crustal growth in Eurasia. Nature 364:299–307.

Shao, J. A.; Liu, F.; Chen, H.; and Han, Q. 2001. Relationship between the Mesozoic magmatism and subduction in Da Hinggan-Yanshan area. Acta Geol. Sin. 75:56–63 (in Chinese with English abstract).

Shinjo, R., and Kato, Y. 2000. Geochemical constraints on the origin of bimodal magmatism at the Okinawa Trough, an incipient back-arc basin. Lithos 54:117–137.

Smith, D. R.; Noblett, J.; Wobus, R. A.; Unruh, D.; Douglass, J.; Beane, R.; Davis, C.; et al. 1999. Petrology and geochemistry of late-stage intrusions of the A-type, mid-Proterozoic Pikes Peak batholith (central Colorado, USA): implications for petrogenetic models. Precambrian Res. 98:271–305.

Sokolov, S. D.; Bondarenko, G. E.; Morozov, O. L.; and Grigor'ev, V. N. 1999. The Asia–Northwestern Pacific transition zone in the Late Jurassic–Early Cretaceous time. Theor. Reg. Prob. Geodyn., p. 30–84 (in Russian).

Song, L. Z.; Zhao, Z. H.; Jiao, G. H.; Sun, P.; Luo, X.; Jiang, X. H.; Wang, Z. H.; Zeng, F. Y.; and Miao, W. D. 2010. Geochemical characteristics of Early Creta-

ceous volcanic rocks from Songliao basin, northeast China, and its tectonic implications. Acta Petrol. Sin. 26:1182–1194 (in Chinese with English abstract).

Song, T. G. 1997. Inversion styles in the Songliao basin (northeast China) and estimation of the degree of inversion. Tectonophysics 283:173–188.

Springer, W., and Seck, H. A. 1997. Partial fusion of basic granulites at 5 to 15 kbar: implications for the origin of TTG magmas. Contrib. Mineral. Petrol. 127:30–45.

Sui, Z. M.; Ge, W. C.; Wu, F. Y.; Zhang, J. H.; Xu, X. C.; and Cheng, R. Y. 2007. Zircon U-Pb ages, geochemistry and its petrogenesis of Jurassic granites in northeastern part of the DaHinggan Mts. Acta Petrol. Sin. 23:461–480 (in Chinese with English abstract).

Sun, M. D.; Chen, H. L.; Zhang, F. Q.; Wilde, S. A.; Dong, C. W.; and Yang, S. F. 2013. A 100 Ma bimodal composite dyke complex in the Jiamusi Block, NE China: an indication for lithospheric extension driven by Paleo-Pacific roll-back. Lithos 162–163:317–330.

Sun, S., and McDonough, W. F. 1989. Chemical and isotopic systematics of oceanic basalts: implications for mantle composition and processes. *In* Saunders, A. D., and Norry, M. J., eds. Magmatism in the ocean basins. Geol. Soc. Lond. Spec. Publ. 42:313–345.

Sylvester, P. J. 1989. Post-collisional alkaline granites. J. Geol. 97:261–280.

Tanaka, T.; Togashi, S.; Kamioka, H.; Amakawa, H.; Kagami, H.; Hamamoto, T.; Yuhara, M.; et al. 2000. JNdi-1: a neodymium isotopic reference in consistency with LaJolla neodymium. Chem. Geol. 168:279–281.

Tao, K.; Niu, F.; Ning, J.; Chen, Y. J.; Grand, S.; Kawakatsu, H.; Tanaka, S.; Obayashi, M.; and Ni, J. 2014. Crustal structure beneath NE China imaged by NECESSArray receiver function data. Earth Planet. Sci. Lett. 398:48–57.

Tomurtogoo, O.; Windley, B. F.; Kröner, A.; Badarch, G.; and Liu, D. Y. 2005. Zircon age and occurrence of the Adaatsag ophiolite and Muron shear zone, central Mongolia: constraints on the evolution of the Mongol-Okhotsk ocean, suture and orogen. J. Geol. Soc. 162: 125–134.

Turner, S. P.; Foden, J. D.; and Morrison, R. S. 1992. Derivation of some A-type magmas by fractionation of basaltic magma: an example from the Padthaway Ridge, South Australia. Lithos 28:151–179.

Wang, F.; Zhou, X. H.; Zhang, L. C.; Ying, J. F.; Zhang, Y. T.; Wu, F. Y.; and Zhu, R. X. 2006*a*. Late Mesozoic volcanism in the Great Xing'an Range (NE China): timing and implications for the dynamic setting of NE Asia. Earth Planet. Sci. Lett. 251:179–198.

Wang, L. W.; Wang, Y.; Yang, J.; Wu, G. Q.; Li, G. Y.; and Sheng, L. 2007. Pre-Mesozoic basement provenance tracing of the Songliao basin by means of detrital zircon SHRIMP chronology. Earth Sci. Front. 14:151–158 (in Chinese with English abstract).

Wang, P. J.; Chen, F.; Chen, S. M.; Siebel, W.; and Satir, M. 2006*b*. Geochemical and Nd-Sr-Pb isotopic composition of Mesozoic volcanic rocks in the Songliao basin, NE China. Geochem. J. 40:149–159.

Wang, P. J.; Liu, W. Z.; Wang, S. X.; and Song, W. H. 2002*a*. $^{40}Ar/^{39}Ar$ and K/Ar dating on the volcanic rocks in the Songliao basin, NE China: constraints on stratigraphy and basin dynamics. Int. J. Earth Sci. 91:331–340.

Wang, P. J.; Ren, Y. G.; Shan, X. L.; Sun, S. B.; Wan, C. B.; and Bian, W. H. 2002*b*. The Cretaceous volcanic succession around the Songliao basin, NE China: relationship between volcanism and sedimentation. Geol. J. 37:97–115.

Wang, T.; Guo, L.; Zheng, Y.; Donskaya, T.; Gladkochub, D.; Zeng, L.; Li, J.; Wang, Y.; and Mazukabzov, A. 2012. Timing and processes of late Mesozoic mid-lower-crustal extension in continental NE Asia and implications for the tectonic setting of the destruction of the North China craton: mainly constrained by zircon U-Pb ages from metamorphic core complexes. Lithos 154:315–345.

Wang, T.; Zheng, Y.; Zhang, J.; Zeng, L.; Donskaya, T.; Guo, L.; and Li, J. 2011. Pattern and kinematic polarity of late Mesozoic extension in continental NE Asia: perspectives from metamorphic core complexes. Tectonics 30. http://dx.doi.org/10.1029/2011TC002896.

Wang, X. G., and Wang, Y. 2007. Zircon SHRIMP U-Pb dating of igneous rocks from the basement of the north belt of the south Songliao basin and its geological significances. Geol. Sci. Technol. Inf. 26:23–27 (in Chinese with English abstract).

Wang, Z. W.; Yang, J. L.; and Gao, R. Q. 1993. Petroleum geology of the Daqing oil field. Petroleum Industry, Beijing (in Chinese with English abstract).

Whalen, J.; Currie, K.; and Chappell, B. 1987. A-type granites: geochemical characteristics, discrimination and petrogenesis. Contrib. Mineral. Petrol. 95:407–419.

Windley, B. F.; Alexeiev, D.; Xiao, W.; Kröner, A.; and Badarch, G. 2007. Tectonic models for accretion of the Central Asian Orogenic Belt. J. Geol. Soc. 164:31–47.

Wolf, M. B., and Wyllie, P. J. 1994. Dehydration-melting of amphibolite at 10 kbar: the effects of temperature and time. Contrib. Mineral. Petrol. 115:369–383.

Wu, F. Y.; Jahn, B. M.; Wilde, S. A.; Lo, C. H.; Yui, T. F.; Lin, Q.; Ge, W. C.; and Sun, D. Y. 2003. Highly fractionated I-type granites in NE China. II. Isotopic geochemistry and implications for crustal growth in the Phanerozoic. Lithos 67:191–204.

Wu, F. Y.; Jahn, B. M.; Wilde, S.; and Sun, D. Y. 2000. Phanerozoic crustal growth: U-Pb and Sr-Nd isotopic evidence from the granites in northeastern China. Tectonophysics 328:89–113.

Wu, F. Y.; Lin, J. Q.; Wilde, S. A.; Zhang, X. O.; and Yang, J. H. 2005. Nature and significance of the Early Cretaceous giant igneous event in eastern China. Earth Planet. Sci. Lett. 233:103–119.

Wu, F. Y.; Sun, D. Y.; Ge, W. C.; Zhang, Y. B.; Grant, M. L.; Wilde, S. A.; and Jahn, B. M. 2011*a*. Geochronology of the Phanerozoic granitoids in northeastern China. J. Asian Earth Sci. 41:1–30.

Wu, F. Y.; Sun, D. Y.; Li, H. M.; Jahn, B. M.; and Wilde, S. 2002. A-type granites in northeastern China: age and

geochemical constraints on their petrogenesis. Chem. Geol. 187:143–173.

Wu, F. Y.; Sun, D. Y.; Li, H. M.; and Wang, X. L. 2001. The nature of basement beneath the Songliao Basin in NE China: geochemical and isotopic constraints. Phys. Chem. Earth A 26:793–803.

Wu, F. Y.; Yang, Y. H.; Xie, L. W.; Yang, J. H.; and Xu, P. 2006. Hf isotopic compositions of the standard zircons and baddeleyites used in U-Pb geochronology. Chem. Geol. 234:105–126.

Wu, H.; Zhang, L.; Wan, B.; Chen, Z.; Zhang, X.; and Xiang, P. 2011*b*. Geochronological and geochemical constraints on Aolunhua porphyry Mo-Cu deposit, northeast China, and its tectonic significance. Ore Geol. Rev. 43:78–91.

Xiao, W. J.; Windley, B. F.; Hao, J.; and Zhai, M. G. 2003. Accretion leading to collision and the Permian Solonker suture, Inner Mongolia, China: termination of the Central Asian Orogenic Belt. Tectonics 22. doi: 10.1029/2002TC001484.

Xu, W. L.; Pei, F. P.; Wang, F.; Meng, E.; Ji, W. Q.; Yang, D. B.; and Wang, W. 2013. Spatial-temporal relationships of Mesozoic volcanic rocks in NE China: constraints on tectonic overprinting and transformations between multiple tectonic regimes. J. Asian Earth Sci. 74:167–193.

Xu, W. L.; Wang, D. Y.; and Wang, S. M. 2000. PTtc model of Mesozoic and Cenozoic volcanisms and lithospheric evolution in eastern China. J. Changchun Univ. Sci. Technol. 20:329–335 (in Chinese with English abstract).

Yamamoto, T. 2007. A rhyolite to dacite sequence of volcanism directly from the heated lower crust: Late Pleistocene to Holocene Numazawa volcano, NE Japan. J. Volcanol. Geotherm. Res. 167:119–133.

Yu, J. J.; Wang, F.; Xu, W. L.; Gao, F. H.; and Pei, F. P. 2012. Early Jurassic mafic magmatism in the Lesser Xing'an-Zhangguangcai Range, NE China, and its tectonic implications: constraints from zircon U-Pb chronology and geochemistry. Lithos 142–143:256–266.

Yu, X.; Xiao, J.; Chen, H. L.; Zhang, F. Q.; Xu, Y.; Dong, C. W.; and Pang, Y. M. 2008. Phanerozoic magmatic events in the basement of Songliao basin: SHRIMP dating of captured zircons from the Yingcheng Formation volcanic rocks. Acta Petrol. Sin. 24:1123–1130 (in Chinese with English abstract).

Yuan, H. L.; Gao, S.; Liu, X. M.; Li, H. M.; Günther, D.; and Wu, F. Y. 2004. Accurate U-Pb age and trace element determinations of zircon by laser ablation-inductively coupled plasma-mass spectrometry. Geostand. Geoanal. Res. 28:353–370.

Zeng, T.; Wang, T.; Guo, L.; Tong, Y.; Zhang, J. J.; Shi, X. J.; Zhang, L.; and Li, Y. F. 2011. Ages, origin and geological implications of Late Mesozoic granitoids in Xinkailing Region, NE China. J. Jilin Univ. 41:1881–1990 (in Chinese with English abstract).

Zhang, F. Q.; Chen, H. L.; Dong, C. W.; Pang, Y. M.; Shu, P.; Wang, Y. L.; and Yang, S. F. 2008*a*. SHRIMP zircon U-Pb geochronology of volcanic rocks and discussion on the geological time of the Yingcheng Formation of the northern Songliao basin. J. Stratigr. 32:15–20 (in Chinese with English abstract).

Zhang, F. Q.; Chen, H. L.; Dong, C. W.; Yu, X.; Xiao, J.; Pang, Y. M.; Cao, R. C.; and Zhu, D. F. 2008*b*. Evidence for the existence of Precambrian basement under the northern Songliao basin. Geol. China 35: 421–428 (in Chinese with English abstract).

Zhang, F. Q.; Chen, H. L.; Yu, X.; Dong, C. W.; Yang, S. F.; Pang, Y. M.; and Batt, G. E. 2011. Early Cretaceous volcanism in the northern Songliao basin, NE China, and its geodynamic implication. Gondwana Res. 19: 163–176.

Zhang, F. Q.; Cheng, X. G.; Chen, H. L.; Dong, C. W.; Yu, X.; Xiao, J.; Xu, Y.; Pang, Y. M.; and Shu, P. 2009. Zircon chronological and geochemical constraints on the Late Mesozoic volcanic events in the southeastern margin of the Songliao Basin, NE China. Acta Petrol. Sin. 45:180–185 (in Chinese with English abstract).

Zhang, F. Q.; Pang, Y. M.; Yang, S. F.; Dong, C. W.; Chen, H. L.; and Shu, P. 2007. Geochronology of zircon SHRIMP, geochemistry and its implication of the volcanic rocks from Yingcheng Formation in depression area, north of Songliao Basin. Acta Geol. Sin. 81:1248–1258 (in Chinese with English abstract).

Zhang, J. H.; Gao, S.; Ge, W. C.; Wu, F. Y.; Yang, J. H.; Wilde, S. A.; and Li, M. 2010. Geochronology of the Mesozoic volcanic rocks in the Great Xing'an Range, northeastern China: implications for subduction-induced delamination. Chem. Geol. 276:144–165.

Zhang, Q., and Li, C. D. 2012. Granites: implication for continental geodynamics. China Land, Beijing (in Chinese with English abstract).

Zhang, Q.; Wang, Y.; Li, C. D.; Jin, W. J.; and Jia, X. Q. 2006*a*. A granite classification based on pressures. Geol. Bull. China 25:1274–1278 (in Chinese with English abstract).

Zhang, Q.; Wang, Y.; Li, C. D.; Wang, Y. L.; Jin, W. J.; and Jia, X. Q. 2006*b*. Granite classification on the basis of Sr and Yb contents and its implications. Acta Petrol. Sin. 22:2249–2269 (in Chinese with English abstract).

Zhao, G. L.; Yang, G. L.; and Fu, J. Y. 1989. Mesozoic volcanic rocks in the central-southern Da Hinggan Ling Range. Beijing Press of Science and Technology, Beijing (in Chinese).

Zhou, L. L.; Zeng, Q. D.; Liu, J. M.; Friis, H.; Zhang, Z. L.; and Duan, X. X. 2013. Geochronology of the Xingshan molybdenum deposit, Jilin Province, NE China, and its Hf isotope significance. J. Asian Earth Sci. 75:58–70.

Zorin, Y. A. 1999. Geodynamics of the western part of the Mongolia-Okhotsk collisional belt, Trans-Baikal region (Russia) and Mongolia. Tectonophysics 306:33–56.